Energy &
Environmental
Science

Accepted Manuscript

This article can be cited before page numbers have been issued, to do this please use: X. Wang, Z. Chen, S. Liu, S. Tu, R. Zhan, L. Wang and Y. Sun, *Energy Environ. Sci.*, 2025, DOI: 10.1039/D4EE06107A.

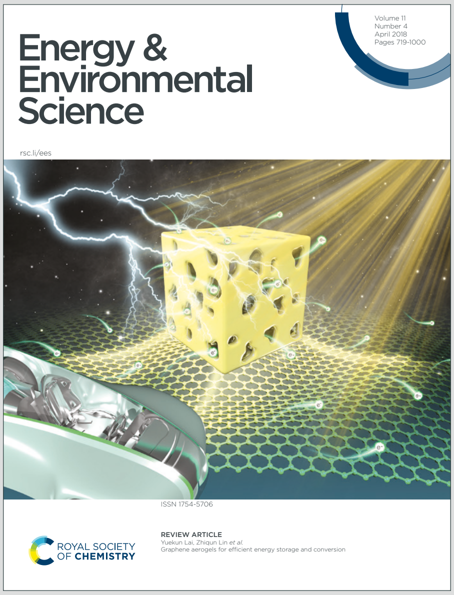
Energy &
Environmental
Science

Volume 11
Number 4
April 2018
Pages 719-1000

rsc.li/ees

ISSN 1754-5706

ROYAL SOCIETY
OF CHEMISTRY

REVIEW ARTICLE
Yuekun Lai, Zhiqun Lin *et al.*
Graphene aerogels for efficient energy storage and conversion

ROYAL SOCIETY
OF CHEMISTRY

rsc.li/ees

View Article Online
DOI: 10.1039/D4EE06107A

Broader Context

The demand for lithium (Li)-based rechargeable batteries with exceptional fast-charging capabilities has surged. However, the sluggish charge transfer kinetics at battery anode poses a significant barrier to achieving this technical requirement. The empirical evidence suggests that the strategic design of the interphase significantly augments the electrochemical reaction kinetics of battery anode materials, concurrently enhancing their fast-charging/discharging performance. The objective of this review is to provide an insightful review on the anode interphase design of Li-based rechargeable batteries for superior fast-charging capability and high energy density, to reveal the categorizations and functions of different interphases, and to offer insights into the future anode interphase design direction and underlying principles. In this review, multiple interphases are categorized into outer/inner interphases based on their physical/chemical environment in batteries. In addition, we will discuss the functions of outer and inner interphase design, including improving the electrochemical reaction kinetics and achieving superior cycling stability, and the interphase design principle for different anode materials is proposed. Finally, after summarizing the current research status and understanding, some perspectives on future development in this area are given.

View Article Online
DOI: 10.1039/D4EE06107A

Anode Interphase Design for Fast-Charging Lithium-Based Rechargeable Batteries

Received 00th January 20xx,
Accepted 00th January 20xx

DOI: 10.1039/x0xx00000x

Xiancheng Wang,[a,§] Zihe Chen,[a,§] Shiyu Liu,[a,§] Shuibin Tu,[a] Renming Zhan,[a] Li Wang,[b] Yongming Sun,[a,*]

High energy density and exceptional fast-charging capability are emerging as critical technical parameters for lithium (Li)-based rechargeable batteries, aimed at meeting the increasing demands of advanced portable electronics, electric vehicles, and grid energy storage systems. However, the sluggish charge transfer kinetics associated with contemporary graphite anodes significantly hinder both the fast-charging performance and overall energy characteristics of existing Li-based rechargeable batteries. As we transition to high-capacity anodes (such as alloying-type and Li metal anodes) for next-generation high-energy-density batteries, their inherent slow electrochemical Li^+/e^- combination rate presents new challenges for fast charging. Furthermore, the significant volume changes that occur during charge and discharge processes contribute to the structural instability of these high-capacity materials and electrodes. This phenomenon also leads to severe side reactions between the active material and the electrolyte, ultimately compromising the electrochemical cycling lifespan. The empirical evidence suggests that the strategic design of the interphase significantly augments the electrochemical reaction kinetics of battery anode materials, concurrently enhancing their structural stability. Nevertheless, a profound understanding of the intricate mechanisms is still lacking, making the establishment of a universal design rule for various anode materials a challenging task. In this review, we categorize the interphases of anode materials into outer and inner interphases based on their physical/chemical environments in batteries. After a comprehensive discussion on the roles and mechanisms of advanced interphases across a range of anode materials, including graphite, alloying-type, and Li metal foil anode materials, we elucidate the principles of outer and inner interphase design, with an emphasis on enhancing their electrochemical reaction kinetics. Several advanced strategies for the design of electrode structures are also proposed to synergistically enhance the Li^+ transport processes. Subsequently, we provide typical examples of advanced interphase design, based on the understanding of the proposed interphase design principles for various anodes. Additionally, we offer a review on the future direction of anode interphase design, aiming at the development of high energy density Li-based rechargeable batteries with superior fast-charging capability and long lifespan.

Introduction

Over the past three decades, lithium (Li)-based rechargeable batteries have undergone rapid development, catering to their application in large-scale energy storage, electric vehicles, and electronic devices.[1-4] Among the performance parameters of these batteries, high energy density and fast-charging capability emerge as two primary objectives in relation to advanced applications.[5-8] Nevertheless, the simultaneous attainment of the two objectives presents substantial challenges. The state-of-the-art graphite anode with Li+ intercalation/extraction mechanism ($Li^+ + e^- + C_6 \leftrightarrow LiC_6$) offers a relatively modest mass specific capacity of 372 mAh g^{-1}, and it brings a moderate energy density of 200-300 Wh kg^{-1} for the current Li-based rechargeable batteries.[9,10] The development of anode materials with higher specific capacity surpassing graphite represents the most promising approach in achieving high-energy-density batteries. This includes alloying-reaction type materials (e.g., Si, P, and Sn, etc) and plating/stripping-type Li metal anode ($Li^+ + e^- \leftrightarrow Li$).[11-13] Typically, Si anode materials can yield a high theoretical specific capacity of 3759 mAh g^{-1}, based on the lithiation product of $Li_{15}Si_4$ ($15Li^+ + 15e^- + 4Si \leftrightarrow Li_{15}Si_4$).[14-16] This is a tenfold increase compared to that of graphite. As illustrated in Fig. 1, the energy density of batteries utilizing such anodes can achieve 300-400 Wh kg^{-1} (using alloying-type anode materials) and even surpass 500 Wh kg^{-1} (using Li metal anode).[17,18] This can be attributed to the incorporation of high-specific-capacity anode materials, which effectively reduces both the anode mass loading and its ratio in full cells. However, the implementation of these advanced anodes encounters significant challenges. Notable volume changes in these anode materials, along with severe side reactions with electrolytes, occur throughout the charge/discharge processes (e.g., approximately 300% for silicon). These phenomena result in particle cracking, delamination of active material layers from current collectors, and the accumulation of unstable solid electrolyte interphase

---

[a] *Wuhan National Laboratory for Optoelectronics, Huazhong University of Science and Technology, Wuhan 430074, China.*
E-mail: yongmingsun@hust.edu.cn
[b] *Institute of Nuclear and New Energy Technology, Tsinghua University, Beijing 100084, China.*

§ *These authors contributed equally to this work.*

Electronic Supplementary Information (ESI) available: [details of any supplementary information available should be included here]. See DOI: 10.1039/x0xx00000x

View Article Online
DOI: 10.1039/D4EE06107A

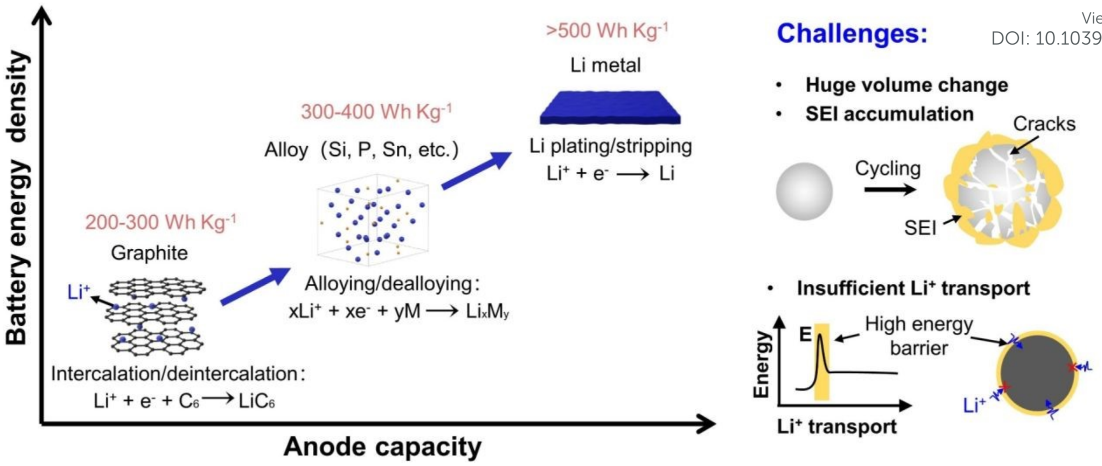

Fig. 1 The advancements and challenges in the development of anode materials for achieving fast-charging Li-based rechargeable batteries with high energy density. Regarding the energy density of batteries, conventional Li-based rechargeable batteries with graphite anodes typically display an energy density within the range of 200 to 300 Wh kg^{-1}. The substitution of graphite with alloying-type anodes can markedly enhance the energy density to between 300 and 400 Wh kg^{-1}. Furthermore, the use of a Li metal anode can facilitate an even higher energy density, exceeding 500 Wh kg^{-1}. The primary challenge linked to graphite anode is the insufficient transport of Li ions at the material/electrolyte interphase. Anodes that possess higher specific capacities grapple with additional challenges, primarily attributed to significant volume changes and an unstable SEI.

(SEI) layers. The impeded movement of lithium ions associated with such SEI formation leads to a decrease in reversible capacity as well as diminished rate performance and fast-charging capabilities of batteries.[19-22] Therefore, future advancements should be pursued through innovative designs aimed at developing advanced anode materials with high specific capacity, stable structures, and rapid charge transfer kinetics. This approach will facilitate the creation of high-energy-density Li-based rechargeable batteries that exhibit exceptional fast-charging capability.

Historically, researches have concentrated on construction of anode interphases to enhance cycling stability and long cycling lifespan.[23-26] However, it has largely neglected the aspects of electrochemical reaction kinetics, resulting in overlooked fast-charging capability. More fundamentally, there is a significant lack of understanding regarding how interphase components and structures influence their functions. It is essential to clarify the design principles of interphases for various anode materials, as this complicates efforts to develop anodes with superior fast-charging capabilities and cycling stability under diverse conditions. While there are several review articles that introduce the design of anode materials for Li-based rechargeable batteries, these studies often focus on different aspects. Some articles provide a comprehensive overview of anode materials, such as graphite, and their role in facilitating fast-charging batteries.[5,7,27,28] Others underscore the significance of material structural design in enhancing cycling stability,[11,18,29] while a separate group of articles is devoted to discussing materials suitable for high-energy-density batteries.[12,17,30] However, a profound discussion and understanding of the anode interphase, which is widely acknowledged as a crucial determinant of a battery's fast-charging capability, is conspicuously absent. Consequently, it is both timely and necessary to review the field of material interphase design for fast charging. This will facilitate a deeper understanding of their potential to address the challenges of sluggish electrochemical reaction kinetics and issues related to anode structural stability.

In this review, we provide a comprehensive elucidation of the different interphases of anode materials based on their physical/chemical environments in batteries, encompassing outer interphase and inner interphase. The outer interphase is defined as the interphase between the active materials and the electrolyte. This particular interphase serves a dual purpose: it physically separates the active materials from the corrosive effects of the electrolyte and facilitates Li^+ desolvation and diffusion across it into the bulk material. Consequently, it plays a pivotal role in dictating the kinetics of electrochemical reactions and the stability of anodes. The inner interphase, on the other hand, is characterized by the encapsulation of the interphase within the anode material, thus achieving direct physical isolation from the electrolyte. The presence of an inner interphase within active materials augments the electrochemical reaction area and enhances the reaction kinetics. We clarify their respective designs and functions to accommodate various material characterizations. For instance, a graphite anode with low volume change and fast Li^+ intercalation reaction can achieve excellent electrochemical performance through effective outer interphase design, resulting in impressive fast-charging/discharging performance and cycling stability. In contrast, high-specific-capacity anodes with unstable structures and slow phase transformation kinetics require careful inner interphase design to improve structural stability and reaction kinetics. We propose design

View Article Online
DOI: 10.1039/D4EE06107A

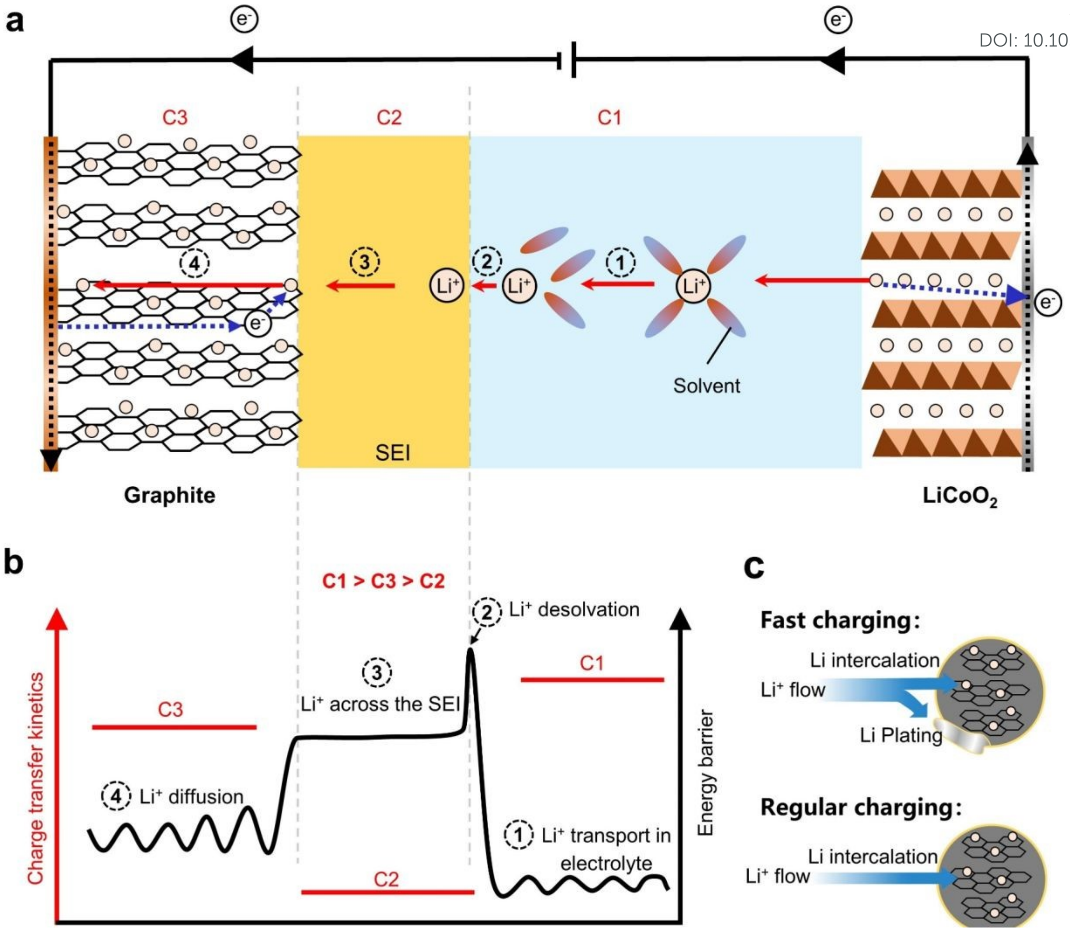

Fig. 2 Charge transfer processes in anode during the battery charging. (a) Charge transfer mechanisms in a $LiCoO_2$||graphite cell during the charging process. (b) Comparison of energy barrier and Li^+ diffusion rates across various processes of the anode. Reproduced with permission.[7] Copyright 2020, Royal Society of Chemistry. The Li^+ desolvation at the material/electrolyte interphase and its subsequent diffusion across it are considered as the most energy-demanding stages throughout the entire charge transfer process. (c) Schematic of the Li^+ intercalation process in the graphite anode under both regular and fast-charging conditions. There is a pronounced likelihood for Li plating to transpire on the surface of the graphite anode under fast-charging condition.

principles and examples for both outer and inner interphases to enhance fast-charging capability and cycling lifespan in Li-based rechargeable batteries. Additionally, we provide insights into the rational design direction and fundamental principles for anode interphase engineering to support broader applications under various operational conditions.

Charge transfer in anode during battery charging

Understanding the charge transfer process in a battery is fundamental for discerning the factors that influence fast-charging performance and guiding anode interphase design. Taking a Li cobalt oxide ($LiCoO_2$)||graphite cell as an example (Fig. 2a), the separation of Li ions and electrons initially occurs at the cathode during the charging process, driven by electric field effects. This process leads to the extraction of Li ions from the cathode materials and their diffusion into the liquid electrolyte, followed by solvation by solvent molecules. The solvated Li ions in the electrolyte then diffuse through the separator towards the anode side. Typically, the transport of solvated Li ions at the anode during the charging process can be categorized into four distinct steps: 1) The movement of solvated Li ions within the liquid electrolyte in the porous electrode structure of the anode. 2) The desolvation of solvated Li ions at the anode material/electrolyte interphase. 3) The translocation of Li ions across the anode material/electrolyte interphase. 4) The diffusion of Li ions into the bulk anode material.[27,31,32] Compared to other processes, the desolvation and subsequent transport of Li ions at the anode material/electrolyte interphase are considerably slower and the most energy-consuming steps in commercial electrodes (Fig. 2b).[7,33] Therefore, it is crucial to develop effective designs for the anode interphase that augment both Li^+ desolvation and transport at this pivotal interphase to achieve high-energy-density Li-based rechargeable batteries with fast-charging capability. Simultaneously, electrons generated by the cathode during the charging process transfer from the external circuit to the anode current collector and subsequently move to the porous active material layer. The combination of Li^+/e^- at the anode material culminates in the completion of the entire

View Article Online
DOI: 10.1039/D4EE06107A

charge process of the batteries. As a result, a continuous lithiation reaction at the anode is facilitated throughout the battery charging process.

The charge transfer process within batteries inherently facilitates rapid electrochemical reaction kinetics, thereby resulting in enhanced fast-charging/discharging performance. The primary factors influencing electron transfer include the electrical conductivity of both current collectors and conductive additives, as well as that of the active materials. In contrast, Li^+ transport processes are governed by more complex variables such as electrolyte composition, pore structure of the electrode, properties of the active material, and characteristics at the anode material/electrolyte interphase. The transport of Li ions to the anode necessitates careful evaluation and analysis during fast-charging operations. This is particularly important given that electron transport through the circuit and current collector occurs at an exceptionally rapid rate. Indeed, this movement at the electrode surpasses that of Li ions. Consequently, under conditions characterized by high current density charging, lithium plating is likely to occur on the surface of graphite anodes once electrons combine with Li ions on the electrode surface due to the relatively slow diffusion rates of Li ions (Fig. 2c).

Interphase categorization of anode materials

This review emphasizes the paramount importance of interphase design in the pursuit of high-energy-density Li-based rechargeable batteries with fast-charging capability. The charging capability of the battery anode is significantly hindered by Li^+ desolvation at the material/electrolyte interphase and Li^+ diffusion through it. Given that the Li+ transport process occurs at the anode material/electrolyte interphase, more focused attention should be directed towards the influence of interphase structure and composition on the Li^+ desolvation and diffusion processes. Historically, research has been centered on designing interphases for high ionic conductivity, with the objective of enhancing the electrochemical performance of various anode materials.[34-37] A few researches investigated the facilitation of Li^+ desolvation process by anode material/electrolyte interphase regulation.[38-40] Thus, the interrelationship between the interphase components and their structural characteristics, along with their roles and mechanisms in enhancing electrochemical reaction kinetics, remains inadequately understood. In this section, we systematically define and categorize various types of interphases while elucidating their respective functions. Furthermore, we propose distinctive design principles for interphases that are specifically tailored to different anode systems, aiming to achieve high energy density and rapid charging capabilities across a diverse range of application scenarios.

Considering the pivotal role of the interphase in facilitating electrochemical reactions and safeguarding active materials against corrosion, we classify the interphases into outer and inner interphases based on their respective physical/chemical environments within batteries (Fig. 3a). The outer interphase denotes the interphase between active materials and the liquid electrolyte. This particular interphase physically segregates the active materials from the corrosive electrolyte. Concurrently, Li^+ desolvation occurs at this interphase and permits Li^+ transport through it, thereby playing a crucial role in determining the electrochemical reaction kinetics and stability of the anodes. It is noteworthy that this interphase can be formed through material interphase engineering and can also be established via in situ electrochemical reactions during the electrochemical formation cycle, namely SEI. On the other hand, the inner interphase is characterized by the interphase being encapsulated within the anode material, thereby achieving direct physical isolation from the electrolyte (Fig. 3b).

The incorporation of multiple interphases can effectively address the significant challenges encountered by battery anodes. It is essential to emphasize that the design of an outer interphase on the graphite anode, which is characterized by high ionic conductivity and rapid Li^+ desolvation capabilities, substantially enhances the kinetics of electrochemical reactions. The rational design of the inner interphase becomes essential for higher-specific-capacity alloy-type anode materials compared with graphite material. Alloy-type active materials often possess slower lithiation/delithiation kinetics as they undergo the initial chemical bonding of the material breaking and the formation of new Li-containing chemical bonds,[41,42] a process that is more energy-consuming than Li intercalation/extraction processes. An enriched inner ionic conductive interphase increases the active area for electrochemical reaction, shortens the charge transport distance in bulk material, thereby improving reaction kinetics at the material-electrolyte interphase (Fig. 3c). Practically, electrode structures are categorized into porous and foil-type structures. Porous electrodes, with rational porosity (e.g., 20-30% for commercial graphite electrodes), offer a unique advantage for solvated Li^+ transport. On the other hand, Li metal foil electrodes comprise a dense structure and planar structure, which presents a very limited accessible surface area to electrolyte for electrochemical reaction. Thus, Li^+/e^- combination and separation only occur at the surface of Li metal foil electrodes accessible to electrolyte. Consequently, it is imperative to construct abundant inner interphases throughout the entire foil to facilitate efficient electrochemical reactions, which necessitate rapid inner Li^+ transport capability and active sites for Li^+/e^- combination. In fact, an internal framework of the active material facilitates interconnected inner interphases, which not only provide a rapid charge transfer pathway but also offer mechanical support to accommodate the volume changes of the active material during the charge/discharge process. Consequently, this internal network can enhance the structural stability of the anode material and increase the availability of active sites for electrochemical reactions. The design of these inner interphases is particularly crucial for Li metal foil anodes, as their high electrochemical reactivity and significant volume

View Article Online
DOI: 10.1039/D4EE06107A

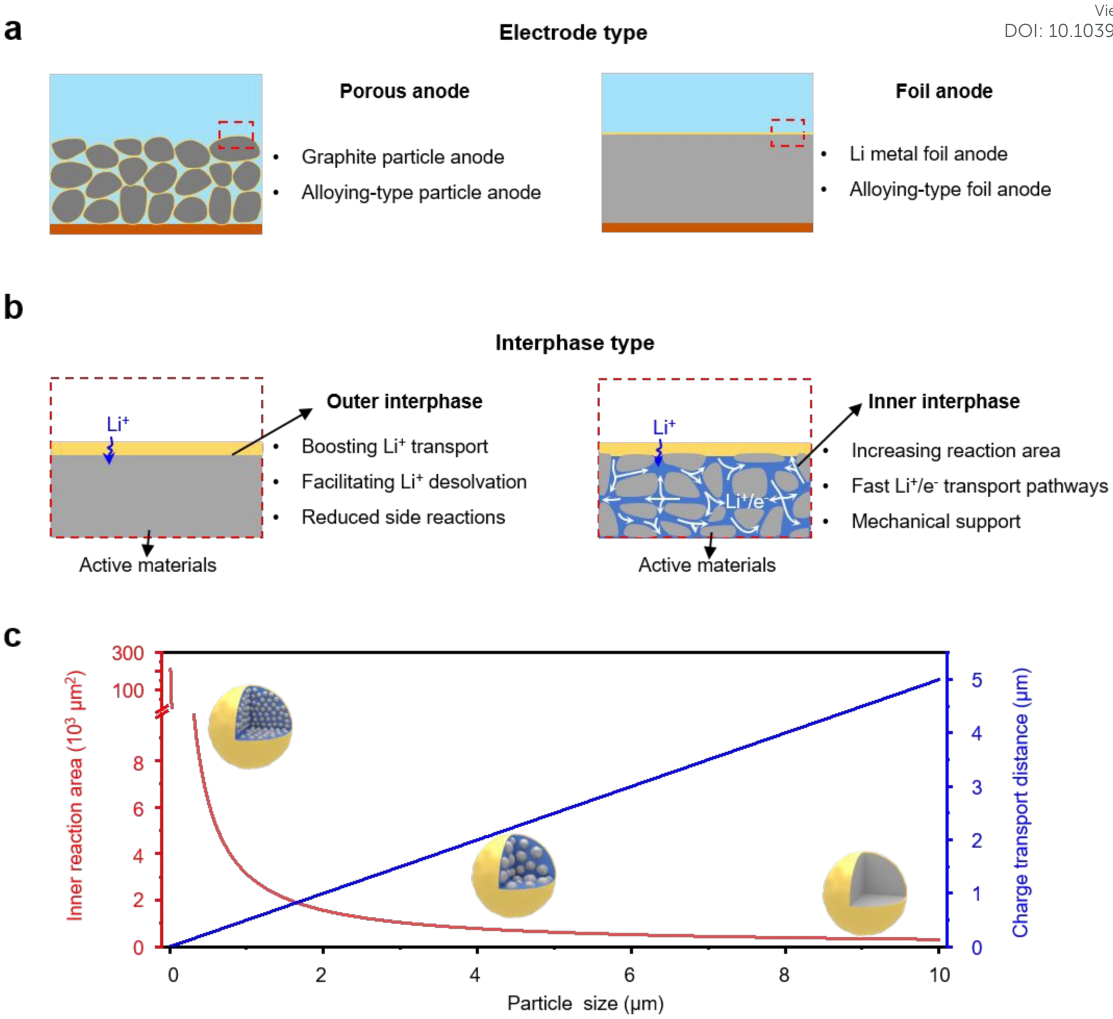

Fig. 3 Schematic of electrode structure and interphase type in anodes. (a) Schematic of electrode types of various anode materials. Porous electrodes are fabricated utilizing particulate active material via a slurry-based process, whereas foil electrodes comprise Li metal foil and alloy-type foils (Sn, Al, Zn, etc). (b) Interphase categorization and roles for various anode materials. (c) The relationship between particle size, charge transport distance, and reaction area in the context of inner interphase design development. The calculations are conducted based on a spherical model with constant overall particle size (10 μm). As the pristine particles transform into smaller-sized secondary particles, they become isolated by an internal charge transport pathway. This transformation results in an increase in the total surface area of the secondary particles, consequently increasing the inner reaction area. Particle size is defined as the diameter of the sphere, while the reaction area corresponds to the sum of the surface areas of all individual particles. The charge transfer distance is defined as half of the particle diameter.

change ratio present considerable challenges in performance. Therefore, we propose that the optimal design principles for the anode interphase should prioritize minimizing the area of the outer interphase while maximizing that of the inner interphase. With the above understanding, a stable outer interphase characterized by a reduced surface area would effectively diminish side reactions with the electrolytes, thereby enhancing cycling stability.

For an electrode with relatively low areal capacity (e.g., <3 mAh cm^{-2}), the slow charge transfer processes at the anode/electrolyte interphase, including Li$^+$ desolvation on the surface and Li$^+$ transport through it, significantly limit its applicability in fast-charging Li-based rechargeable batteries. In contrast, electron transfer at the anode occurs at an ultrafast rate, resulting in Li plating as electrons combine with concentrated Li ions on the surface of the anode material. Consequently, it is essential to design an outer interphase that enhances both the desolvation process of Li ions and their diffusion across this interphase to improve the fast-charging capability of such anodes.

Outer interphase design of anode materials

For an electrode with relatively low areal capacity (e.g., <3 mAh cm^{-2}), the slow charge transfer processes at the anode/electrolyte interface, including Li$^+$ desolvation on the surface and Li$^+$ transport through it, significantly limit its applicability in fast-charging Li-based rechargeable batteries. In

contrast, electron transfer at the anode occurs at an ultrafast rate, leading to Li plating when electrons combine with concentrated Li ions on the surface of the anode material. Therefore, designing an outer interphase that enhances both the Li$^+$ desolvation process and their diffusion across the outer interphase is crucial for improving the fast-charging/discharging capability of such anodes.

1. Boosting Li$^+$ transport across the outer interphase

The transport of Li ions across the outer interphase precedes its migration into the bulk material,, which is situated between the active material and the liquid electrolyte. This interphase is noteworthy due to its potential for creation through material interphase engineering. Besides, it can also be in situ generated via the decomposition of meticulously designed electrolyte on the material surface, a phenomenon known as the regulated SEI. High-ionic-conductive components of interphase can facilitate Li$^+$ diffusion across it with low energy barrier (Fig. 4a). Thus, high ionic conductive species were widely considered into anode interphase design.[43-46] Li phosphide (Li_3P) has garnered substantial attention in the annals of battery research, primarily due to its long-standing consideration as a solid electrolyte candidate, attributable to its high ionic conductivity.[47-49] Incorporating Li_3P into the outer interphase with a thin thickness can enhance Li$^+$ transport across it and synergistically improve the fast-charging/discharging performance of various anode materials. The feasibility of a Li_3P-based anode interphase was investigated. A red phosphorus (P) interphase, approximately 15 nm thick, was constructed on Si particles. During the initial lithiation processes, the P surface layer underwent in situ conversion into a Li_3P layer (with an average lithiation potential of ~0.7 V *vs.* Li$^+$/Li) prior to the conversion of Si into Li_xSi alloy (< 0.5 V *vs.* Li$^+$/Li). It is noteworthy that the delithiation potential of Li_3P (> 1 V *vs.* Li$^+$/Li) is significantly high, ensuring that it remains stable within the cut-off voltage range typical for regular anodes (< 1 V *vs.* Li+/Li), including graphite and silicon anodes (Fig. 4b). Thus, the Li_3P nanoshell remained stable after the formation cycle and does not participate in lithiation/delithiation during subsequent battery charge/discharge cycling. Figs. 4c, d depict the transmission electron microscopy (TEM) images, accompanied by the corresponding mapping images of Si and P, following a complete charge/discharge cycle in a half cell with a charge voltage of 1 V (*vs.* Li$^+$/Li). Importantly, a Li_3P interphase was well maintained on the material surface subsequent to the delithiation operation of the Si anode, a phenomenon attributable to the high delithiation voltage of Li_3P. This observation underscores the commendable stability of the Li_3P interphase during cycling in a regular anode cut-off voltage range (0-1 V *vs.* Li$^+$/Li). Moreover, the solid-state nature of Li_3P effectively isolated the active silicon species from corrosive electrolytes. As a result, a stable *in situ* electrochemically formed Li_3P outer interphase functions as an efficient barrier that enhances rapid Li$^+$ transport while mitigating side reactions between Si and the electrolyte. Consequently, this Li$^+$ conductive Li_3P interphase significantly improves cycling stability (Fig. 4e). The fast-charging/discharging performance of Si-based anodes was also improved. The Si/P anode demonstrated remarkable capacities of 2193, 2043, 1685, 1383, and 912 mAh g^{-1} at discharge rates of 0.05, 0.1, 0.5, 1 and 2 *C*, respectively. In contrast, the pure Si anode displayed a rapid capacity decay, registering a mere 158 mAh g^{-1} at a discharge rate of 1 *C* (Fig. 4f).[50]

In addition to the Li_3P-based interphase, other components exhibiting high ionic conductivity were also investigated to enhance fast-charging/discharging performance and cycling stability of various anode materials. For example, a MgH_2 outer interphase was design on Si particle, which underwent in situ electrochemical lithiation into LiH and Li_xMg alloy, effectively enhancing the lithiation kinetics of Si anode.[51] Additionally, a Li_3N-rich outer interphase was successfully constructed through the design of a Si@$MgSiN_2$ anode material (Fig. 4g). The high ionic conductivity from Li_3N significantly improved the fast-charging/discharging performance of Si anode (Fig. 4h).[52] Furthermore, the formation of outer interphases containing of $Li_4Ti_5O_{12}$,[53] Li_3PO_4,[54] and various Li alloys (e.g., Li-Sb,[55] Li-Ga,[56] Li-Bi,[35] Li-In (Fig. 4i)[57]) served a similar purpose by facilitating Li$^+$ transport process across these interphases. This improvement contributed significantly to the fast-charging capability observed in Li-based rechargeable batteries. Recently, a layer of MoO_x-MoN_x, exhibiting superior Li$^+$ diffusion capability, was engineered onto graphite surface, which facilitated a high specific capacity of 340.3 mAh g^{-1} at 6 *C*, even after 4000 cycles.[58] Al_2O_3-decorated graphite anode was designed with the intention of improving reaction kinetics. Molecular dynamics (MD) simulations demonstrated that incorporated Al_2O_3 nanoparticles could disrupt charge distributions within the anode/electrolyte layer, creating what can be described as an "interfacial highway" that facilitated efficient Li$^+$ transport at the Al_2O_3/electrolyte interphase.[59] This strategy offered novel insights into interfacial design for advancing fast-charging Li-based rechargeable batteries.

In addition to the design of interphase components, electrolyte engineering has emerged as an effective strategy for enhancing the fast-charging and discharging performance, as well as the cycling stability of anode materials. This enhancement is primarily achieved through the formation of a SEI (outer interphase) that is rich in inorganic components, which significantly improves ionic conductivity and mechanical stability when compared to conventional SEI dominated by organic components. An electrolyte with $Cu(NO_3)_2$ additive was developed, which facilitated the formation of Li_3N-based SEI with high Li$^+$ conductivity.[60] A high-concentration electrolyte consisting of 6 M lithium bis(fluorosulfonyl)imide (LiFSI) in 1,3-dioxolane (DOL) with 2wt% $LiNO_3$ additive enabled the formation of LiF/Li_3N-rich SEI (Figs. 4j, k). Such a SEI favored remarkable mechanical strength and rapid Li$^+$ transport capability, thereby extending the fast-charging/discharging performance of Si anode (Fig. 4l).[61] The Si anode, when cycled

View Article Online
DOI: 10.1039/D4EE06107A

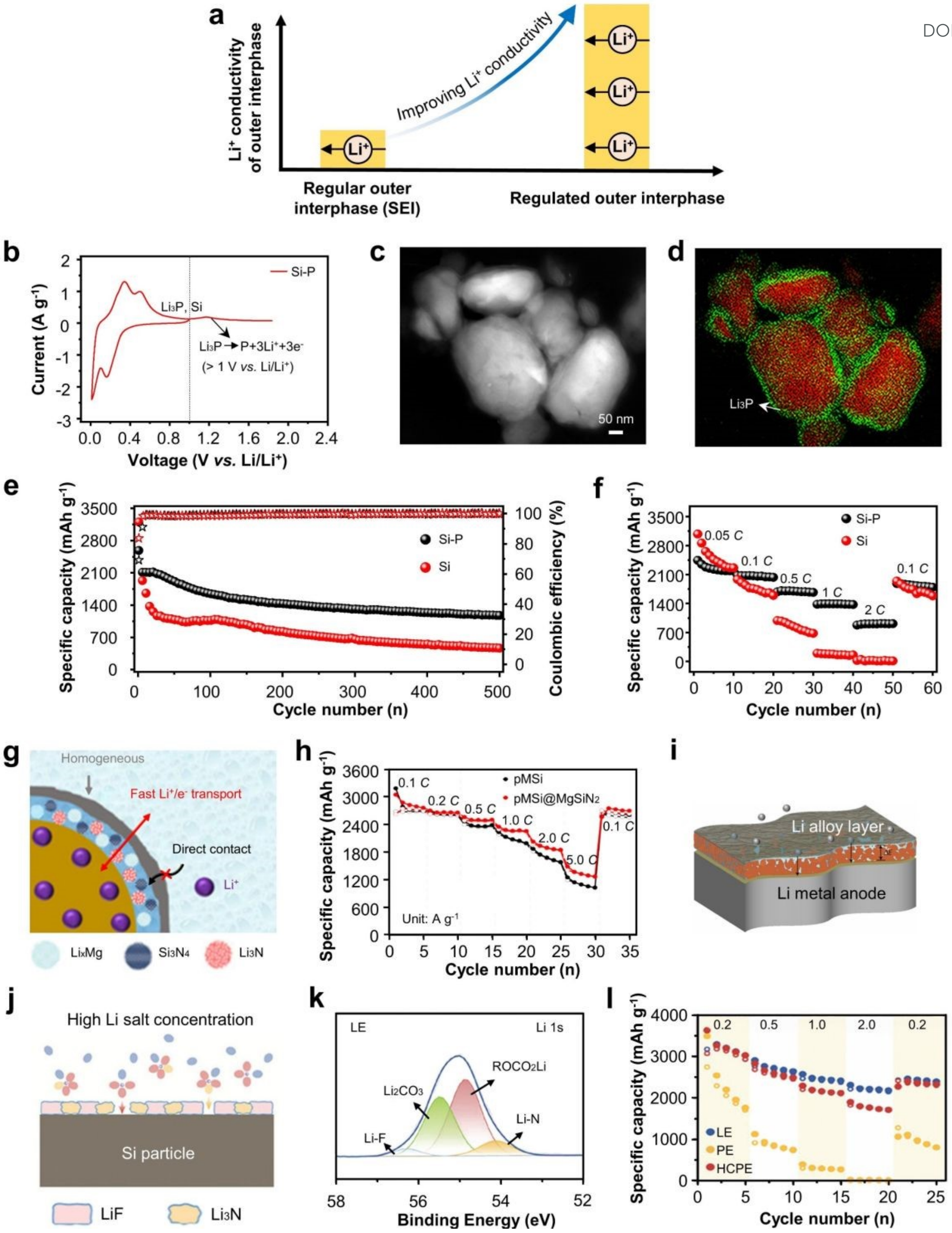

Fig. 4 Outer interphase design for enhancing Li⁺ transport. (a) Schematic of high-ionic-conductivity outer interphase in enhancing Li⁺ transport. (b) 1st cyclic voltammograms (CVs) curves of Si-P anode at a scan rate of 0.1 mV s^{-1}. The delithiation potential of Li_3P surpasses 1 V (*vs.* Li⁺/Li), a characteristic that guarantees its stability throughout the cycling process. (c) TEM images of Si-Li_3P following the first discharge/charge cycle in half cell configuration, with a delithiation cut-off voltage of 1 V (*vs.* Li⁺/Li), and (d) the corresponding elemental mapping image of Si and P elements. Owing to the moderately high delithiation voltage of Li_3P, a stable Li_3P interphase endures on the Si surface post-charging. (e) Cycling performance and (f) fast-charging performance for both the Si-P and pristine Si anodes. Reproduced with permission.[50] Copyright 2021, SpringerLink. (g) Schematic of the formation of a Li_3N-rich outer interphase on the $MgSiN_2$ modified Si anode. $MgSiN_2$ undergoes *in situ* lithiation into Li_xMg, Si_3N_4 and Li_3N, a process that enhances the Li⁺ transport at the interphase. (h) Charge/discharge measurement at various current densities of Si anodes with and without $MgSiN_2$ outer interphase modification. Reproduced with permission.[52] Copyright 2024, Elsevier. (i) Schematic of the Li alloy layer on the Li metal anode to enhance Li⁺ transport. Reproduced with permission.[57] Copyright 2017, Springer Nature. (j) Schematic of the SEI composition on the Si anode in high-concentration electrolyte conditions, and (k) the corresponding high-resolution Li 1s X-ray photoelectron spectroscopy spectrum. A Li_3N-rich SEI was established on the Si anode, thereby augmenting its fast charging/discharging capability. (l) Charge/discharge measurement at various current densities for Si anodes tested across different electrolytes. Reproduced with permission.[61] Copyright 2023, John Wiley & Sons.

View Article Online
DOI: 10.1039/D4EE06107A

in the aforementioned electrolyte, demonstrated a high capacity of 2210 mAh g^{-1} at 2 *C*. This is in stark contrast to the counterpart, which lost virtually all of its capacity at the same test current density. Despite of the great progress in the electrolyte design for tailoring the SEI characteristics, further improvement in electrochemical performance necessitate the synergistic approach that combines both materials interphase design and electrolyte optimization.

2. Facilitating Li$^+$ desolvation at the outer interphase

The Li$^+$ desolvation process also takes place at the outer interphase. Recent studies have identified the optimization of the outer interphase composition as a crucial research direction for enhancing the kinetics of electrochemical reaction. This was predicated on the verification that a composition possessing robust bonding interactions with Li ions can expedite efficient Li$^+$ desolvation processes (Fig. 5a). Utilizing a combination of MD simulations and density functional theory (DFT), it was discovered that among the conventional SEI compositions, inorganic species, including LiF, Li_2O, and Li_2CO_3, exhibited a lower coordination number and a higher affinity for Li ions in comparison to the organic species (Fig. 5b). Notably, Li_3P distinguished itself by possessing the lowest coordination number and the highest affinity for Li ions, suggesting that Li_3P required minimal energy for the desolvation of Li ions. By virtue of its efficient desolvation capability coupled with high ionic conductivity, Li_3P emerged as a promising candidate for an ideal component of SEI, aiming at promoting Li$^+$ transport at the material interphase. A red P interphase, characterized by a uniform structure and an ultrathin thickness of approximately 4.4 nm, was successfully fabricated on the graphite surface through a S-assisted vapor deposition approach (Fig. 5c, defined as P-S-graphite anode). The red P interphase at the graphite surface underwent an in situ transformation into a continuously crystalline Li_3P interphase with a thickness of ~8 nm during the battery formation cycle (Fig. 5d). This Li_3P-dominated SEI notably facilitated rapid Li$^+$ desolvation processes and enhanced electrochemical reaction kinetics (Fig. 5e). $LiNi_{0.6}Co_{0.2}Mn_{0.2}O_2$ (NCM622)||P-S-graphite (anode, ~2.3 mAh cm^{-2}) pouch cell achieved 80% of the capacity after just 6 minutes of charging under current conditions corresponding to 10 *C*. In stark contrast, NCM622||graphite pouch cell exhibited only 57.4% of capacity under identical test conditions at 10 *C*. Significantly, Ah-level NCM622||P-S-graphite laminated pouch cell demonstrated an impressive capacity retention of 82.9% after 2000 cycles with a charging current of 6 *C* (1 *C* = 1 A), which is unprecedented in Ah-level pouch cells. In stark contrast, NCM622||graphite pouch cell showed only 46% capacity retention under same test conditions at a charge rate of 6 *C* (Fig. 5f).[62]

The effective promotion of the Li+ desolvation process by Li_3P species was also investigated extensively. A dense layer of black P (BP) was composited onto the graphite surface through a high-energy ball milling method, referred to as BP-Gr. The in situ formation of a thin Li_3P-containing interphase layer (Fig. 5g) during the anode lithiation processes significantly facilitated the Li$^+$ desolvation process. Employing a propylene carbonate (PC)-based electrolyte, the cells demonstrated impressive electrochemical performance under low temperature and fast-charging conditions. A high capacity retention of 70% (compared to room temperature) was achieved at -20 °C with a charging rate of 4 *C* (Fig. 5h). Additionally, a capacity retention of 65% was attained at -40 °C when charged at 0.05 *C* (Fig. 5i).[63] Besides Li_3P, Li_3PO_4 also shown promise in facilitating Li$^+$ desolvation processes. Compared to other SEI components such as Li_2CO_3 and LiF, Li_3PO_4 possessed the lowest work function and easily donates electrons, which enhanced the adsorption efficiency for solvated Li ions and facilitates their desolvation.64

The effectiveness of the Li_3P-containing interphase for fast charging was also demonstrated in Si-based anodes. In addition to its role in promoting Li$^+$ desolvation, its interaction with electrolyte components was investigated and a robust SEI dominated by binary Li_3P/LiF species was achieved, which enabled both the fast-charging capability and cycling stability of high-specific-capacity anodes. A SiO_x@P anode was designed and the interaction between P and the FEC solvent (electrolyte additives) was revealed. FEC exhibited significant reduction on the surface of the SiO_x@P, enabling the production of LiF together with the formation of Li_3P during the formation cycle of batteries (Fig. 5j). As demonstrated, a NCM622||SiO_x@P pouch cell exhibited exceptional fast-charging capability, achieving 86.5% and 81.2% of its capacity (compared to the charging capacity measured at 0.2 *C*) at 4 *C* (charging for 15 minutes) and 6 *C* (charging for 10 minutes), respectively. In contrast, the NCM622||SiO_x pouch cell reached only 41.4% of its capacity under similar conditions at 6 C as compared to that tested at 0.2 C. Further evaluations of the SiO_x@P anode within a 1.3 Ah pouch full cell demonstrated both superior fast-charging capability and cycling stability under fast-charging conditions. Specifically, it exhibited a high capacity retention of ~83.8% after undergoing successive cycles at a charging rate of 4 *C* over 250 cycles (Fig. 5k).[65] This finding provided new insights into the employment of the outer interphase design to optimize the SEI formation processes, aiming at advancing high-energy-density Li-based rechargeable batteries with improved fast-charging performance.

The operational conditions of the cell, such as temperature and pressure, can significantly influence the interaction between the material and the electrolyte, subsequently affecting the resulted SEI. Further analysis and discussion are conducted based on relevant research. Prior studies have indicated that an increase in temperature rises tends to form anion-dominated solvation sheaths within the electrolyte, leading to the formation of inorganic-rich SEI. However, at elevated temperatures, a greater number of solvents are likely to be reduced on the anode surface, resulting in a significant increase in organic substances within the interphase and inevitably augmenting the thickness of the SEI.[66, 67] Therefore, by meticulously regulating and optimizing the temperature

View Article Online
DOI: 10.1039/D4EE06107A

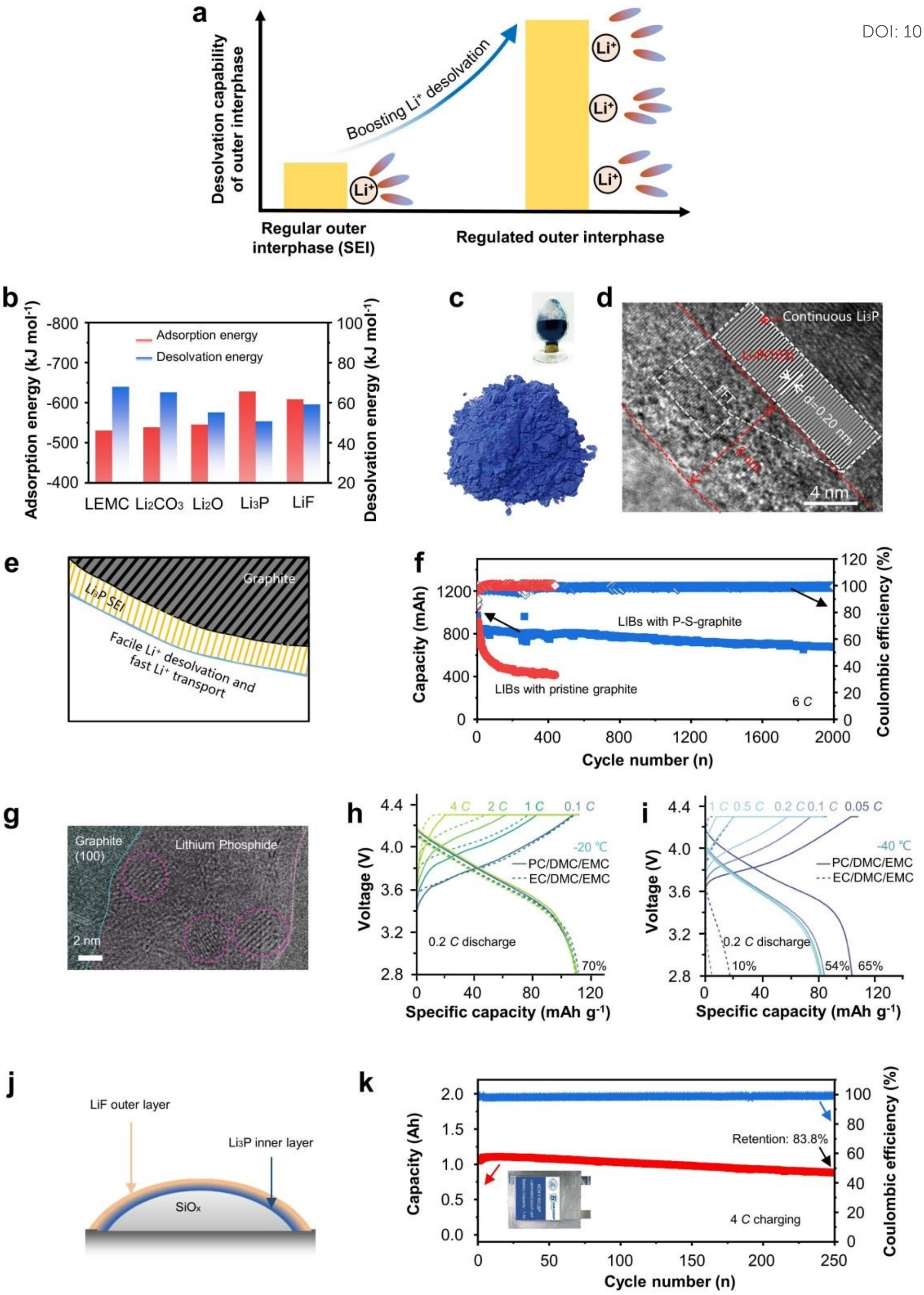

Fig. 5 Outer interphase design for facilitating Li$^+$ desolvation. (a) Schematic of outer interphase design for facilitating Li$^+$ desolvation. (b) Comparison of Li$^+$ affinity energy and desolvation barrier of different SEI components. Li_3P demonstrated the highest Li$^+$ affinity energy and the lowest desolvation barrier in comparison to other species, thereby suggesting its significant role in facilitating the desolvation of Li ions. (c) Optical photographs of the as-prepared P-S-graphite anode. (d) High-resolution TEM (HRTEM) images of the cycled P-S-graphite anode featuring a Li_3P outer interphase, and (e) the corresponding schematic of the cycled P-S-graphite anode. Reproduced with permission.[62] Copyright 2023, Springer Nature. Following cycling, a continuous Li_3P interphase was formed on the P-S-graphite anode, which significantly enhanced the fast desolvation and transport of Li ions across it. (f) Cycling performance for NCM622||P-S-graphite pouch cell at fast-charging rate of 6 C. (g) HRTEM images of BP-Gr anode after lithiation, resulting in a Li_3P-containing outer interphase formation. (h) Charge/discharge curves of BP-Gr anode at -20 °C and (i) -40 °C conditions. Reproduced with permission.[63] Copyright 2023, John Wiley & Sons. (j) Schematic of SEI formation on the SiO_x@P anode surface. Upon cycling, a dual-layer SEI, predominantly constituted of LiF and Li_3P, was established on the surface of the SiO_x@P anode. (k) Cycling performance for NCM622||SiO_x@P laminated pouch cell at fast-charging rate of 4 C. Reproduced with permission.[65] Copyright 2023, Royal Society of Chemistry.

View Article Online
DOI: 10.1039/D4EE06107A

during the battery formation cycle, it is feasible to achieve a SEI that is rich in inorganic species and exhibits a thin profile. Pioneering research has been conducted on Li metal anodes, focusing on the effects of pressure on the components and structure of SEI. Under relatively low pressure, the morphology of Li deposits displayed irregularities, with the SEI primarily composed of organic components. Conversely, elevated pressure significantly enhanced the uniformity of Li deposits and led to the formation of an inorganic species-dominated SEI. This phenomenon can largely be attributed to the increased participation of anions in the electrolyte reduction process under high pressure.[68, 69]

Inner interphase design of anode materials

1. Increasing inner reaction area

Although significant advancements have been made in the design of outer interphases, considerable challenges associated with the sluggish reaction kinetics of alloying-type and Li metal anodes necessitate a more refined approach to the design of inner interphases, in addition to outer interphases. Extensive research has demonstrated that the use of high-specific-capacity anodes introduces new challenges, including slow phase transformation kinetics and substantial volume expansion. These factors ultimately lead to a diminished fast-charging and discharging capability, as well as degradation of the electrode or material structure after a certain number of cycles. Here, we highlight the potential of inner interphase design. The inner interphase is characterized by its encapsulation within the anode material, a feature that enables it to physically isolate itself directly from the electrolyte. The unique configuration of a cross-linked inner interphase facilitates high material utilization, accelerates electrochemical reaction kinetics, and ensures long-term stability for these high-capacity anodes. This endeavor should encompass the creation of an abundant contact area between the active material and the functional phase available for electrochemical reactions. This should be complemented by an interconnected framework that facilitates rapid Li^+/e^- transport and accommodates volume expansion while preserving structural stability (Fig. 6a).

Red P was incorporated into the nanopores of micrometer-sized porous carbon particles, constructing a red P/C composite, while allowing a red P-free carbon layer at the outer interphase of the composite (Figs. 6b, c). The encapsulation of red P within carbon nanoshells effectively mitigated its direct interaction with the electrolyte, thereby suppressing side reactions and stabilizing the SEI. Furthermore, the interconnected carbon network facilitated rapid electron transport throughout the composite particle. It is noteworthy that hard carbon species are renowned for their exceptional ionic conductivity, positioning them as superior materials for fast-charging anode construction. Consequently, Li^+ transport within the composite was significantly enhanced. This innovative design, characterized by a stable outer interphase in conjunction with a closed inner interphase, enabled outstanding electrochemical performance, encompassing both excellent fast-charging capability and long-term cycling stability. Fig. 6d presented a comparison of the charging/discharging performance among the P/C, commercial graphite, and $Li_4Ti_5O_{12}$ electrodes, each with an identical high areal capacity of 3.5 mAh cm^{-2} (tested at 0.5 mA cm^{-2}). It is notable that the graphite electrode exhibited significant capacity decay, losing nearly all capacity under a charging current density of 2 mA cm^{-2}. In contrast, the P/C electrode demonstrated a capacity retention of 92% at 2 mA cm^{-2}, and retained 84% and 44% of its initial capacity when subjected to charging current densities of 3 and 5 mA cm^{-2}, respectively. These results significantly exceeded the corresponding values for $Li_4Ti_5O_{12}$ (91%, 71%, and 36%), which is generally regarded as the most successful fast-charging anode.[70]

Besides the P/C composite anode, various inner interphase designs were implemented in alloy-type anodes to enhance their structural stability and accelerate the electrochemical reactions. In a typical procedure, a Si/C composite anode, exhibiting a pomegranate-like structure, was prepared. This design incorporated a cross-linked carbon network to augment electrochemical reactions, while the external carbon layer effectively mitigated side reactions between the active material and the electrolyte.[71] A Si-nanolayer-embedded graphite/carbon hybrid (SGC) was developed,[72] characterized by Si nanolayer both on the graphite surface and within the inner pores, along with an outer carbon coating layer (Fig. 6e). This structure provided abundant pathways for Li^+/e^- transport and accommodated the volume expansion of the Si anode. The SGC anode exhibited a high capacity retention of ~95% and ~50% (relative to the capacity at 0.2 *C*) at 3 *C* and 5 *C*, respectively, thereby demonstrating superior fast charging/discharging performance. In contrast, the Si/graphite (Si/G) anode displayed a mere ~10% capacity retention when tested at 5 *C* (Fig. 6f). A coral-like network structure was proposed to improve the fast-charging capability of the cell with a Si anode. The resultant anode exhibited a cross-linked network configuration in which carbon was coated on coral-like porous silicon nanowires. The interconnected carbon layer facilitated a rapid charge transport pathway while the porous structure of silicon provided space for volume expansion.[73] Additionally, other inner interphase designs, such as Si/Fe_2O_3/carbon nanotube composite,[74] macropore-exploited graphite/Si composite,[75] and liquid metal/Si composite[76] were also demonstrated significant effectiveness in enhancing the fast-charging capability of Li-based rechargeable batteries. In a brief conclusion, these innovative approaches to inner interphase design significantly contributed to establishing frameworks that promoted fast Li^+/e^- transport, increased contact areas for electrochemical reactions, and provided adequate space for accommodating subsequent volume expansions.

2. Regulating charge transport pathway within anode particle

In addition to the design of the inner interphase aimed at enhancing the internal reaction area, regulating the orientation

View Article Online
DOI: 10.1039/D4EE06107A

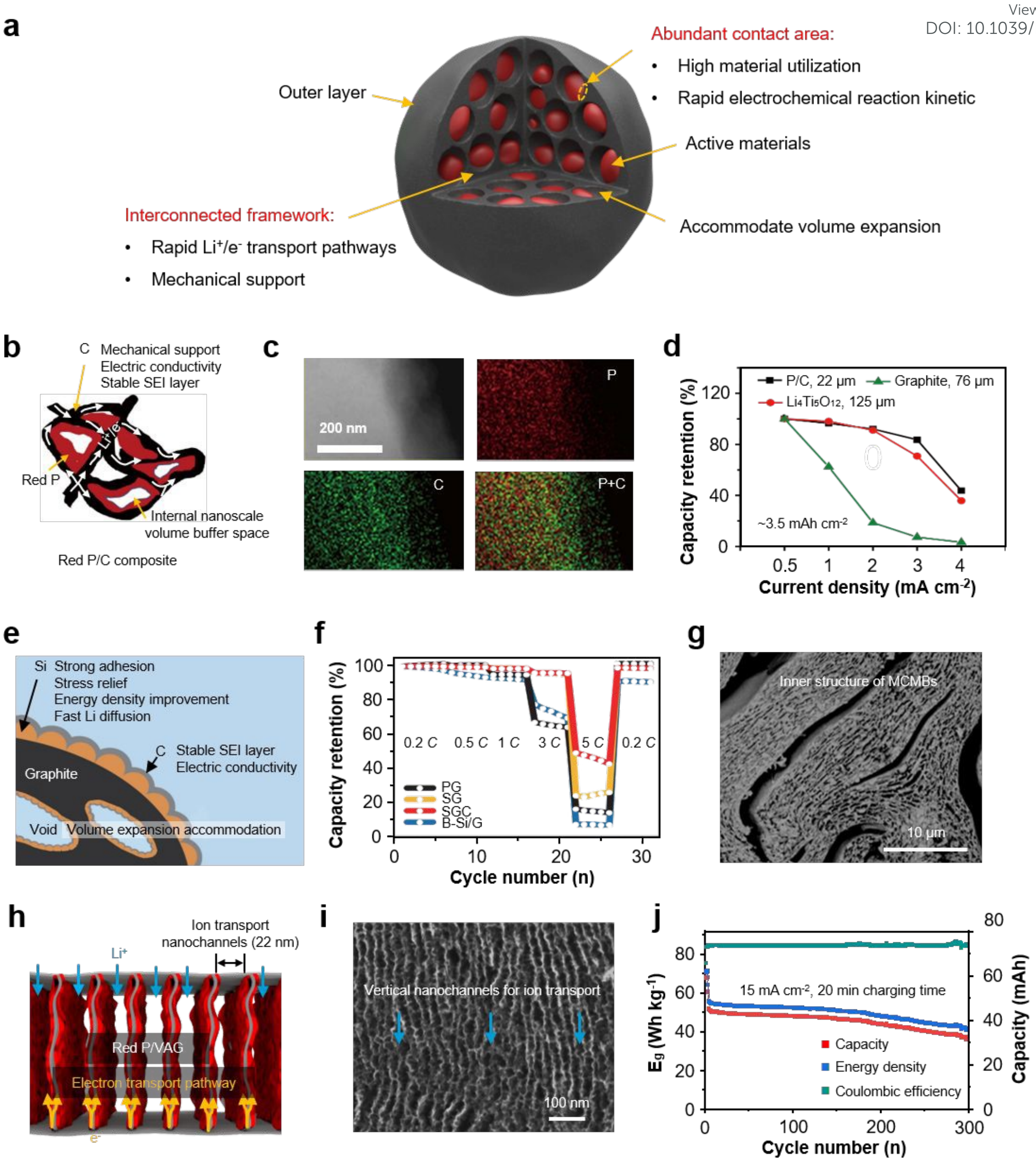

Fig. 6 Inner interphase design for increasing inner reaction area and charge transport pathway. (a) Schematic of the design principles and functions of the inner interphase. (b) Schematic of the red P/C composite anode. Red P was incorporated into the nanopores of micrometer-sized porous carbon particles. (c) TEM images along with corresponding element mapping for the P/C composite anode. (d) Comparison of fast-charging/discharging performance among red P/C, graphite, and $Li_4Ti_5O_{12}$ at a same areal capacity of 3.5 mAh cm^{-2}. Reproduced with permission.[70] Copyright 2019, Elsevier. (e) Schematic of the SGC anode. (f) The comparison of fast-charging/dischrging across various Si and graphite composite anodes. Reproduced with permission.[72] Copyright 2016, Springer Nature. (g) Scanning electron microscopy (SEM) images showcasing the internal structure of MCMBs. Reproduced with permission.[77] Copyright 2014, Elsevier. MCMB exhibited a vertically oriented Li^+ diffusion pathway within a single particle, thereby reducing the Li^+ diffusion distance. (h) Schematic and (i) SEM images of the internal architecture of the red P/VAG anode. The vertical nanochannels fostered low tortuosity for Li^+ transport within the electrode. (j) Cycling performance for NCM622||red P/VAG pouch cell subjected to a high charging current density of 15 mA cm^{-2}. Reproduced with permission.[79]

of charge transport within the particles has proven to be an effective strategy for achieving superior fast-charging capabilities. Typically, meso-carbon microbeads (MCMB) possess a vertically oriented Li^+ diffusion pathway within a single particle (Fig. 6g).[77,78] This orientation significantly reduced the Li^+ diffusion distance compared to regular artificial graphite with disordered inner Li^+ diffusion pathway orientation, thereby achieving superior fast-charging/discharging performance. The mechanism for charging capability improvement was also applicable to the construction of a composite anode with both higher specific capacity of materials and higher areal capacity of the electrode. A chunk composite particle with active material filled inner vertical nanochannels was proposed, and such a particle structure could even support a single layer particle electrode with very high areal capacity and fast-charging capability. The advantage of single-layer particles was its significantly reduced interparticle resistance, which was typically encountered in conventional electrodes with particle stacks. Experimentally, red P was filled into a vertical aligned graphene framework (defined as red P/VAG electrode) with a particle size of ~60 µm and nanochannels of ~22 nm (Figs. 6h, i). These nanochannels promoted low tortuosity for Li+ transport within the electrode. Importantly, encapsulating active red P within graphene effectively reduced the external direct contact area between red P and the liquid electrolyte. The synergistic effects of lower interparticle resistance and tortuosity, more inner reaction interphase, and fewer outer interphase contributed to the accelerated electrochemical reactions in the red P/VAG electrode with a high areal capacity of ~5.6 mAh cm^{-2} (evaluated at 1 mA cm^{-2}) and a high specific capacity of 1011 mAh g^{-1} based on the total mass of the composite. As a result, the red P/VAG electrode (~5.6 mAh cm^{-2}) showed a high capacity retention of 71.4% even at a high tested current density of 8 mAh cm^{-2}, while graphite anode (~5.6 mAh cm^{-2}) tested at same conditions showed low capacity retention of 7%. Such a red P based composite anode was paired with NCM622 cathode for full pouch cell assembly. The NCM622||red-P/VAG pouch full cell tested under fast-charging conditions exhibited a high energy density of 308 Wh kg^{-1} and 792 Wh L^{-1} with a charging time of 20 minutes. Furthermore, after 300 cycles, the cell maintained 76.6% of its initial energy density, thereby demonstrating its practical value under fast-charging conditions (Fig. 6j). These results underlined both the feasibility and practicality of constructing an inner charge transport pathway and regulating oriented particles to achieve simultaneous targets regarding high energy density as well as fast-charging capability in Li-based rechargeable batteries.[79]

Facilitating Li$^+$ transport within the electrode

1. Tortuosity regulation of the electrode

Augmenting the active mass loading of the anode can effectively reduce the weight ratio of inert components in batteries, such as current collectors and separators, thereby enhancing the overall energy density. In the short term, this strategy demonstrates good compatibility with existing battery processing procedures, offering a viable opportunity for rapid implementation within the current industry. However, increasing mass loading directly results in greater electrode thickness, which inevitably hampers Li$^+$ transport across the depth of the electrode. Consequently, elevated electrode mass loading heightens the risk of Li plating, particularly under conditions of fast charging or low-temperature applications (Fig. 7a). As reported previously, the amount of plated metallic Li progressively increased as the areal capacity of the graphite anode was elevated from 2.2 mAh cm^{-2} to 3.3 mAh cm^{-2} and then to 4.4 mAh cm^{-2} under a moderate charging current at 1.5 *C*.[80,81] Therefore, the design aimed at enhancing the Li$^+$ transport capability within the porous structure of the electrode is of vital importance for achieving a fast-charging anode, particularly for those with high mass loading.

The conventional electrode possesses a porous structure consisting of randomly stacked active particles, resulting in a tortuous pathway for Li$^+$ transport across the thickness from the surface to the bottom of the electrode. Reducing the tortuosity of the electrode represents an effective approach to shorten the Li$^+$ transport distance within the electrode.[82] Various methods have been employed to construct electrode architecture for this purpose. For instance, magnetic Fe_3O_4 modified graphite was prepared, allowing for controlled active particle orientation under applied magnetic fields during electrode fabrication (Fig. 7b). This process yielded a graphite electrode with reduced tortuosity, thereby facilitating rapid Li$^+$ transport through its pores and thus improving the fast-charging/discharging capability.[83] Although the low tortuosity and regular graphite electrodes showed a similar capacity of ~390 mAh g−1 at 0.1 *C*, a high capacity of 150 mAh g^{-1} was achieved at 1 C for the low-tortuosity graphite electrodes, which was higher than the value of 50 mAh g^{-1} of the reference (Fig. 7c). A graphite electrode with vertical micrometer-scale pores was developed using a laser-patterning technique (Fig. 7d), significantly enhancing Li$^+$ transport within the electrodes. The excellent fast-charging capability of such a graphite anode was successfully verified in an Ah-class pouch cell.[84] As demonstrated, the cell with laser-patterned treated graphite as anode delivered a stable cycle for 100 cycles with a high capacity retention of ~ 90% at 6 *C* (fast charging for 10 minutes), while the cell with pristine graphite anode showed fast capacity degradation within 20 cycles and low capacity retention of 60% (Fig. 7e). Additionally, a freeze tape casting strategy was employed to decrease the tortuosity of the electrode.[85] Vertically aligned channels with a size of ~10 µm were formed within a graphite electrode through ice crystal formation via freezing treatment and sublimation in the vacuum drying process. The resulting graphite anode possessed highly oriented vertical channels perpendicular to the current collector, enabling an efficient fast-charging capability.

2. Li$^+$ transfer number regulation of the electrode

Besides the tortuosity regulation, increasing Li+ transfer number of the Li$^+$ conductive medium has been verified as another effective approach for improving the Li$^+$ diffusion capability across the electrode depth.[86-88] In a regular electrode, liquid electrolyte with high Li$^+$ conductivity but low Li$^+$ transfer number is filled into the porous electrode structure and works as the Li$^+$ diffusion medium.[89-92] An alternative Li$^+$ transport mode within electrode was proposed, which introduced a new Li$^+$ transport pathway by employing solid electrolyte with higher

View Article Online
DOI: 10.1039/D4EE06107A

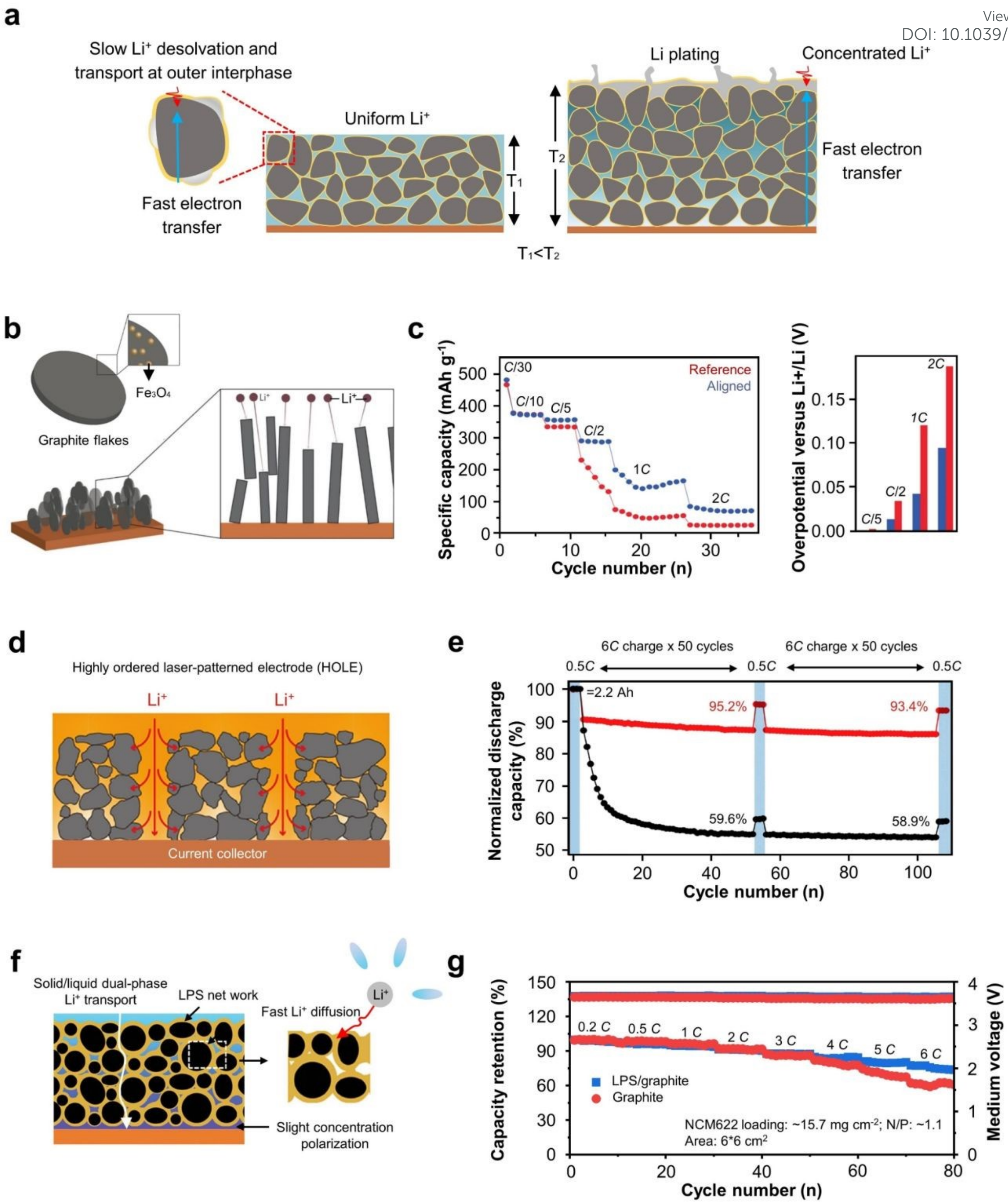

Fig. 7 Regulation of electrode tortuosity and Li⁺ transfer number. (a) Schematic of Li plating on thin and thick graphite electrodes. The insufficient Li⁺ diffusion capability across the electrode depth would cause low active material utilization and Li plating for thick electrode under fast-charging conditions. (b) Schematic of magnetic field modulation for the Fe_3O_4 modified graphite electrode with orientation. Upon the application of a magnetic field, the tortuosity of the electrode decreased. (c) Charging/discharging performance of the oriented Fe_3O_4 modified graphite anode. Reproduced with permission.[83] Copyright 2016, Springer Nature. (d) Schematic of a graphite anode with vertical Li⁺ transport channels achieved through laser-patterning techniques. (e) Fast-charging performance comparison between full cells utilizing regular graphite anode and graphite anode with vertical Li⁺ transport channels. Reproduced with permission.[84] Copyright 2020, Elsevier. (f) Schematic of Li⁺ transport within the LPS/graphite electrode with high transfer number. A hybrid liquid/solid Li⁺ transport mechanism demonstrated the benefits of both liquid and solid electrolytes, thereby promoting an enhanced Li⁺ diffusion capability. (g) Fast-charging capability for the NCM622||LPS/graphite pouch cell. Reproduced with permission.[93] Copyright 2024, John Wiley & Sons.

Li+ transfer number into regular electrode. Such a hybrid liquid/solid Li⁺ transport mechanism displayed both the advantages of liquid and solid electrolytes and enabled enhanced Li+ diffusion capability. Experimentally, a cross-linked

Li_3PS_4 (LPS) solid electrolyte network was established within a graphite anode via a regular slurry procedure and the LPS/liquid electrolyte in electrode exhibited a similar Li^+ conductivity to liquid electrolyte and but significant apparent Li^+ transfer number of 0.68, which was significantly higher than the value of 0.32 observed for conventional liquid electrolytes (Fig. 7f). Consequently, the LPS/graphite electrode alleviated Li^+ concentration gradients, enhanced Li^+ transport capability at electrode levels, and improved the fast-charging capability. When paired with a high mass loading NCM622 cathode (15.7 mg cm^{-2}), cells utilizing LPS/graphite anodes demonstrated 91.3%, 84.8% and 77.5% of their designed capacity (~3.1 mAh cm^{-2}) when charged at 2 *C* (30 minutes) , 4 *C* (15 minutes), and 6 *C* (10 minutes), respectively. In contrast, pouch cells containing pristine graphite anode achieved only approximately 60.1% capacity at a charging rate of 6 *C*, accompanied by poorer cycling stability (Fig. 7g).[93]

3. Increasing inner reaction area of foil-type anode

Foil-type electrodes exhibit a significantly reduced electrochemical reaction area compared to porous particle electrodes, as only the top surface of the foil electrode that is accessible to the electrolyte participates in the electrochemical reactions. The limited electrochemical reaction area, combined with the slow Li^+ diffusion behavior of Li metal foil electrodes, results in inferior electrochemical reaction rates and promotes the growth of Li dendrites. This presents a significant obstacle to achieving optimal fast-charging capabilities and cycling stability in batteries.[94-96] The transformation of the electrochemical reaction location from the surface of the electrode to the bulk of the foil electrode can not only suppress the corrosion by the electrolyte but also increase the electrochemical reaction area. Introducing a framework with high Li^+/e^- conductivity within the Li metal foil electrode divides the bulk into micro-reaction zones, provides abundant built-in pathways for efficient Li^+/e^- diffusion within the electrode, and significantly improves the electrochemical reaction kinetics (Fig. 8a).

A $Li/Li_{22}Sn_5$ composite foil was prepared through a straightforward repeated calendering and rolling process involving Li and Sn foil as the raw materials. This composite was characterized by a Li embedded within a three-dimensional nanostructured $Li_{22}Sn_5$ network with high hybrid Li^+/e^- conductivity and its abundant contact area with metallic Li. As expected, the $Li/Li_{22}Sn_5$ foil exhibited impressive fast-charging/discharge capability, demonstrating stable Li plating/stripping at 30 mA cm^{-2} and 5 mAh cm^{-2} with an overpotential as low as 20 mV sustained over 200 cycles in carbonate electrolyte (Fig. 8b).[97] The Li/LiZn[98] and $Li/LiNO_3$[99] composite anodes were fabricated to establish a rapid Li^+ transport framework. This framework was designed to enhance the kinetics and uniformity of electrochemical reactions. The overarching objective of these approaches was to engineer a Li metal anode characterized by superior cycling stability and fast charging/discharging capability.

Furthermore, the synchronous introduction of LiF to produce a $Li/Li_{22}Sn_5$/LiF composite foil electrode showed ultraslow electrode corrosion during electrochemical cycling, besides its superior fast-charging/discharge capability. Due to the solubility of LiF in ethylene carbonate (EC) (5.5 g L^{-1}) and fluoroethylene carbonate (FEC) (3.3 g L^{-1}), LiF within the composite foil dissolved into the electrolyte, yielding Li ions and F^- ions. When saturation occurred during the dissolution of LiF, $[LiF]_n$ clusters formed, subsequently leading to reprecipitation of LiF on the surface of the Li metal composite foil. This process resulted in a dense, LiF-dominated outer interphase on Li metal anode (Fig. 8c). A symmetric cell composed of $Li/Li_{22}Sn_5$/LiF||$Li/Li_{22}Sn_5$/LiF demonstrated remarkable cycling stability over 1600 hours when tested at 1 mA cm^{-2} and 2 mAh cm^{-2} in a carbonate electrolyte, while the pure Li electrode failed within 300 hours. The fast-charging/discharging performance of the Li metal full cells, featuring $Li/Li_{22}Sn_5$/LiF as anode, was markedly enhanced in comparison to that paired with pure Li. When paired with a $LiCoO_2$ cathode, the full cell incorporating a $Li/Li_{22}Sn_5$/LiF anode demonstrated a remarkable capacity of 3 mAh cm^{-2} at 0.2 *C* (1 *C* = 200 mA g^{-1}), and delivered approximately 83% capacity retention at a charge rate of 2 *C*. In sharp contrast, cells equipped with a pure Li anode only retained only about 50% of the capacity under the identical conditions.[100] A $Li/Li_{22}Sn_5/Li_2S$ composite was also prepared to enhance the electrochemical performance of Li metal anode. In the designed configuration, lithiophilic Li_2S species utilized their high Li^+ adsorption energy to guide preferential Li nucleation, thereby preventing inhomogeneous Li^+ distribution. Simultaneously, the electron-conductive $Li_{22}Sn_5$ framework, engineered with an optimal Li^+ diffusion energy barrier, facilitated efficient charge transport kinetics (Fig. 8d). This synergistic interplay suppressed localized Li^+ aggregation and eliminated hotspots during operation.[101]

It is noteworthy that the composite anode also exhibited robust mechanical characteristics and facilitated superior processability for the Li metal anode.[102-104] A Li/Li_3P (LLP) composite foil was successfully fabricated through mechanical kneading processes involving red P and metallic Li with a thickness below 15 μm. The mechanical durability and processability of the composite foil were enhanced by the uniform dispersion of ionically conductive Li_3P nanoparticles within the matrix. Also, the cycling stability of the LLP anode was ensured by the abundant Li_3P/Li inner contact interphase for fast electrochemical reaction.[105] In addition to Li_3P, analogous second-phase strengthening strategies were corroborated in Li/Ag and Li/AgF anodes. Typically, the incorporation of Ag into the Li matrix markedly enhanced the mechanical strength (Fig. 8e).[106] Moreover, a Li/AgF composite foil exhibited high processability, culminating in the successful fabrication of a 5 μm-thick ultrathin Li metal composite anode (Fig. 8f).[107] These instances underscore the substantial potential of Li metal composite anodes in augmenting both the electrochemical performance and energy density of batteries.

View Article Online
DOI: 10.1039/D4EE06107A

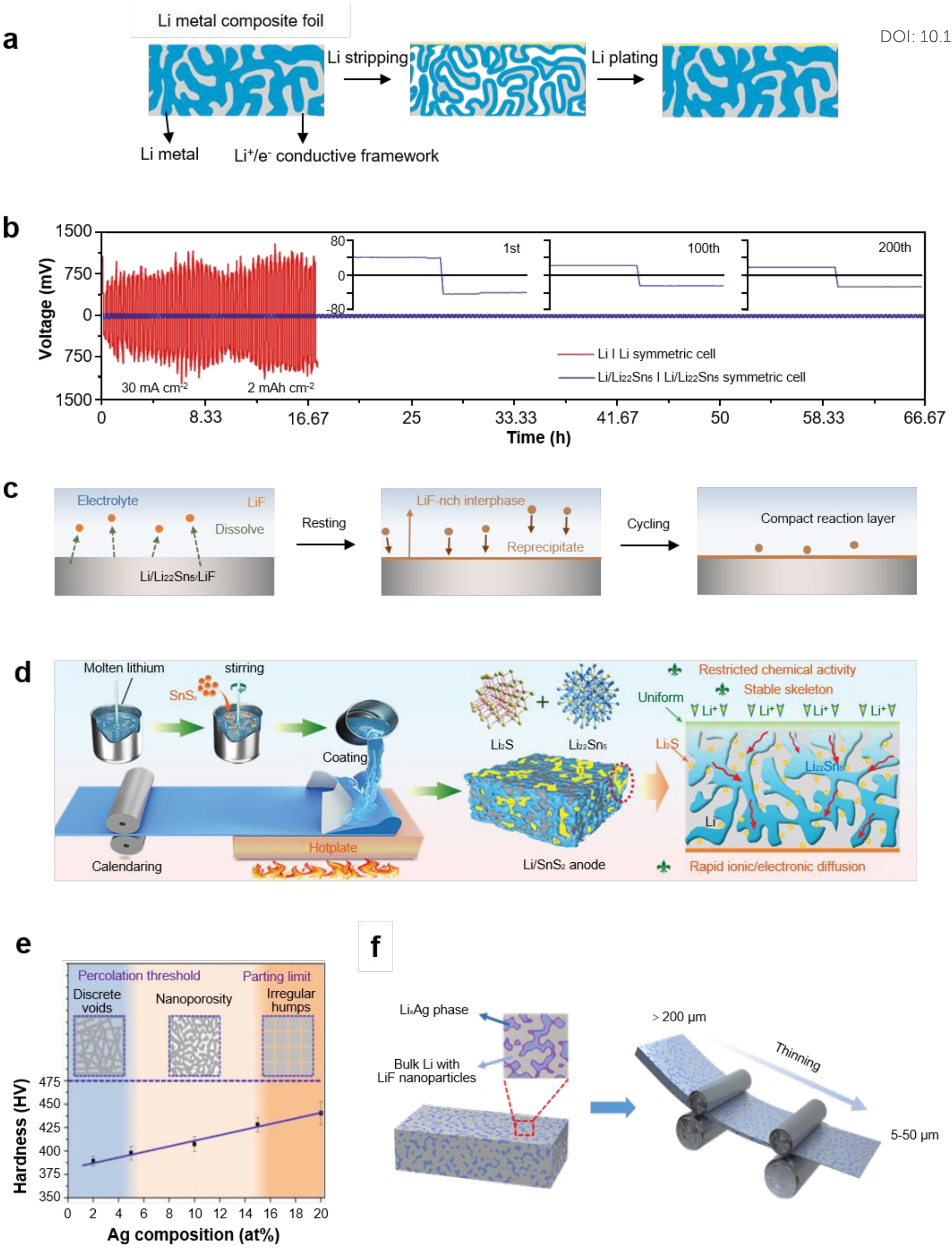

Fig. 8 Increasing the inner reaction area of Li metal foil anodes. (a) Schematic of Li stripping and plating behavior in the Li metal composite foil anode. The integration of a Li^+/e^- conductive network can effectively augment the inner electrochemical reaction area, thereby enhancing the kinetics of electrochemical reactions. (b) Time-voltage profiles for both $Li/Li_{22}Sn_5||Li/Li_{22}Sn_5$ and Li||Li symmetric cells at 30 mA cm^{-2} and 5 mAh cm^{-2}.[97] (c) Schematic of the dissolution-reprecipitation mechanism of LiF for building an anticorrosion $Li/Li_{22}Sn_5/LiF$ anode. Reproduced with permission.[100] Copyright 2023, John Wiley & Sons. (d) Schematic of the synthesis and structure of the $Li/Li_{22}Sn_5/Li_2S$ composite foil. The *in-situ* lithiation reaction of SnS_2 with molten Li culminated in the formation of a $Li_{22}Sn_5$ alloy and Li_2S. Reproduced with permission.[101] Copyright 2024, John Wiley & Sons. (e) The hardness versus Ag content plot of the Li/Ag composite anode. Reproduced with permission.[106] Copyright 2021, John Wiley & Sons. (f) Schematic of the synthesis and structure of the Li/AgF composite foil. The *in-situ* lithiation reaction of AgF with molten Li resulted in the formation of Li-Ag and LiF composite. The mechanical strength of the Li/AgF composite anode was significantly bolstered by the formation of Li-Ag and LiF, facilitating the straightforward preparation of thin Li foils with controllable thickness through a mechanical rolling process. Reproduced with permission.[107] Copyright 2023, American Chemical Society.

View Article Online
DOI: 10.1039/D4EE06107A

Challenges for the practical implementation of advanced interphase design

While the current interphase design strategy has substantially enhanced the fast charge/discharge performance of the anode, the path towards practical application remains fraught with challenges. Factors pertaining to manufacturing, including cost and scalability, warrant careful consideration. For instance, the use of high-performance interphase materials (such as carbon nanotubes and single-atom coatings) and intricate processes (like atomic layer deposition and chemical vapor deposition) considerably escalate manufacturing expenses. These preparation procedures necessitate stringent atmospheric control or specialized equipment, both of which exhibit poor compatibility with the existing battery industry. Moreover, the employment of organic solvents or high-temperature processes (such as high-temperature carbonization for material interphase configuration) may exert an environmental toll. Consequently, it becomes imperative to contemplate the development of suitable technological processes and the selection of abundant, low-cost raw materials for interphase design. Beyond cost and scalability, the long-term cycling stability of the anode under fast charging operation is a critical consideration. The cyclical rupture and regeneration of the SEI during the cycling process can induce continuous active Li loss and an increase in interfacial impedance for Li^+ transport, particularly in high-specific-capacity anodes such as Si-based materials. Simultaneously, the substantial volume expansion of the electrode materials can undermine the integrity of the interphase layer. This degradation may trigger localized electrolyte decomposition and performance decay, ultimately leading to mismatches at the interphase structure and a decline in cycling stability. Therefore, when designing the interphase, it is crucial to prioritize enhancing its resilience and accommodating the volume expansion that occurs during the lithiation of the anode by incorporating sufficient space.

Simultaneously, the multifaceted coupling effect of the electrode must be taken into account, encompassing the synergistic influence of the interphase, morphology, and porosity. The demand for high areal capacity of the electrode leads to an increase in mass loading. However, excessively thick electrodes can elongate Li^+ transport pathways, thereby escalating polarization. For instance, although the SEI exhibits superior Li^+ transport characteristics, an electrode porosity of less than 20% can obstruct electrolyte penetration and significantly diminish the Li^+ diffusion capability within the thick electrode. In addition to the low-tortuosity electrode design, a gradient porosity design can effectively strike a balance between mass loading and porosity: a high porosity (e.g., ~40%) of the surface layer of the electrode facilitates Li^+ transport, while a denser arrangement of active materials at the bottom augments the energy density of the battery. During the research process, it is vital to distinguish the impact of interphase and electrode structural factors on electrochemical performance. This can be evaluated through comparative experiments. For instance, by maintaining a constant electrode structure (such as identical porosity), the performance of batteries with various interphase modifications can be compared to assess the individual contribution of the SEI. Alternatively, by keeping the interphase design of the active material consistent (for example, constructing the same outer interphase), one can adjust the porosity of the electrode (e.g., 20% *vs.* 40%) to quantify the influence of electrode structure on the electrochemical performance.

Conclusions and perspectives

The development of Li-based rechargeable batteries with high energy density and rapid charging capability has become an urgent priority to address the ever-increasing demand for applications. In this review, we summarize the advancements in anode interphase designs aimed at achieving fast-charging Li-based rechargeable batteries. This includes a focus on both existing graphite anode materials and next-generation anode materials with high specific capacities, such as alloying-type and Li metal anodes. We classify the interphases into outer and inner interphases according to their function and physical/chemical environment. The rational design of outer interphase can reduce Li^+ desolvation energy, tailor the SEI, and facilitate Li^+ transport through it. Furthermore, stabilization of the outer interphase between active material/electrode and electrolyte during cycling is crucial to suppress side reactions and minimize active Li consumption. A robust inner interphase with enhanced conductivity provides abundant active sites and increases the electrochemical reaction area and the interconnected conductive framework embedded within the bulk particle provides rapid inner charge transport pathways, which together significantly improve the fast-charging capability of batteries. Our investigation underscores the importance of increasing the inner interphase while stabilizing the outer interphase to achieve fast-charging Li-based rechargeable batteries with both high energy density and extended cycling lifespan. The instances cited in the text, which included a range of interphase design strategies and principles, as along with the corresponding material systems and their realized fast charging/discharging capabilities, are exhaustively outlined in Table 1.

Despite the considerable advancements achieved, the progression towards fast-charging and high-energy-density Li-based rechargeable batteries technologies requires considerable continuous effort. In this context, we outline the primary challenges and propose strategic directions for their practical application through advanced designs of both inner and outer interphases:

(1) The development of an outer interphase that combines facile Li^+ desolvation with superior ionic conductivity remains a primary objective, yet it still poses significant challenges. While various surface coating technologies and electrolyte engineering have been validated as effective approaches,

View Article Online
DOI: 10.1039/D4EE06107A

Table 1 Anode interphase design principles and the corresponding performance outcomes.

Design principles	Materials/electrodes	Performance
Boosting Li$^+$ transport across the outer interphase	Si-P	912 mAh g^{-1} at 2 C
	Si@MgSiN$_2$	1275 mAh g^{-1} at 5 C
	Graphite@MoO$_x$-MoN$_x$	340.3 mAh g^{-1} at 6 C (4000 cycles)
	Si in high-concentration electrolyte	2210 mAh g^{-1} at 2 C
Facilitating Li$^+$ desolvation at the outer interphase	P-S-graphite	80% of the capacity (2.3 mAh cm^{-2}) at 10 C (full cell)
	SiO$_x$@P	81.2% of the capacity (compared to 0.2 C) at 6 C (full cell)
Increasing inner reaction area by inner interphase design	P/C composite	84% of the capacity (3.5 mAh cm^{-2}) at 3 mA cm^{-2}
	SGC anode	50% of the capacity (compared to 0.2 C) at 5 C
Regulating charge transport pathway within anode particle	Red P/VAG anode	71.4% of the capacity (5.6 mAh cm^{-2}) at 8 mA cm^{-2}
Electrode design	Magnetic Fe$_3$O$_4$ modified graphite	150 mAh g^{-1} at 1 C
	Laser-patterned treated graphite	90% of the initial capacity at 6 C (full cell)
	LPS/graphite electrode	77.5% of the capacity (3.1 mAh cm^{-2}) at 6 C (full cell)
Increasing inner reaction area of foil-type anode	Li/Li$_{22}$Sn$_5$ composite foil	30 mA cm^{-2} and 5 mAh cm^{-2} with an overpotential as low as 20 mV, 200 cycles
	Li/Li$_{22}$Sn$_5$/LiF composite foil	1 mA cm^{-2} and 2 mAh cm^{-2}, 400 cycles

elucidating the impact of the component composition and texture of the outer interphase on Li$^+$ transport behavior at the electrode surface has become an urgent task. Consequently, the implementation of various novel experimental methods is indispensable for rational design at the fundamental level. Future research could incorporate *in-situ* characterization techniques and multi-dimensional spectroscopy to monitor the real-time evolution of interphases, such as the dynamic formation and degradation of the SEI, thereby unveiling the microscopic mechanisms of Li$^+$ desolvation and transport in conjunction with simulations. The analysis of the spatial distribution of interfacial chemical composition and the alterations in the coordination environment of Li ions can provide empirical support for the design of interphases with high ionic conductivity and the enhancement of the Li$^+$ desolvation process.

(2) One should pay attention to the interaction between the outer interphase and electrolyte, since the reaction between active materials and electrolyte stands as one main reason for materials corrosion and performance decay, accounting for the long-term cycling stability of batteries. Enhancing the comprehension of the interaction between the outer interphase and electrolyte is essential for advancing battery technology. This involves investigating how various interphase materials influence SEI formation and its property, including Li$^+$ desolvation, charge transfer mechanisms, and mechanical durability. Furthermore, examining the effects of temperature, pressure, and additional environmental factors on this interaction can yield significant insights into improving battery efficiency and longevity. Equally important, the exploration of advanced techniques for characterizing and manipulating the outer interphase could provide a pathway towards understanding the chemical and electrochemical behavior at the material-electrolyte interphase. This could further lead to the development of innovative strategies aimed at enhancing the performance of lithium-based rechargeable batteries.

(3) While the construction of an inner reaction interphase and the embedding of charge transport pathways within the bulk active material directly facilitate rapid electrochemical reaction kinetics, it is crucial to meticulously balance the ratio of active material to inert material. This balance is necessary to achieve a trade-off between high active material loading and the reaction kinetics of anode material, and thus the energy density and fast-charging capability of batteries. Furthermore, for those high-capacity active materials that undergo significant volume expansion during the charge/discharge process, it is essential to maintain an inner void space to buffer volume

View Article Online
DOI: 10.1039/D4EE06107A

changes and construct a mechanically robust framework for better material stabilization, thereby ensuring the long-term cycling stability of the anode.

(4) It is imperative to monitor the evolution of the designed interphases over extended electrochemical cycling, encompassing both the outer and inner interphases. We emphasize the significance of the physical and chemical stability of these interphases within the battery environment. To this end, the exploration of both in situ and ex situ measurement approaches is recommended. This monitoring process involves tracking and analyzing changes in both the structure and composition of cycled interphases. Subsequently, insights gained from understanding the mechanisms underlying interphase evolution during cycling can inform design strategies, thereby mutually optimizing electrochemical performance.

(5) The development of anode materials with intrinsically high specific capacity and superior fast charge/discharge capability is crucial. The selection of suitable anode materials, which inherently possess high specific capacity and excellent rate capability, is of paramount importance. For example, the high specific capacity of red P, coupled with its moderately high work potential and the high ionic conductivity of Li_3P, makes red P-based materials particularly apt as anode materials for fast-charging lithium-based rechargeable batteries. When these materials are incorporated with both inner and outer interphase designs, they can achieve enhanced charging/discharging capability and an extended cycling lifespan.

Notes

The authors declare no competing interests.

Acknowledgements

The authors would like to thank the support by National Natural Science Foundation of China (No. 52072137).

References

1 S. Chu, Y. Cui and N. Liu, *Nat. Mater.* 2016, **16**, 16-22.
2 M. S. Whittingham, *Chem. Rev.* 2020, **120**, 6328-6330.
3 J. Xiao, F. Shi, T. Glossmann, C. Burnett and Z. Liu, *Nat. Energy* 2023, **8**, 329-339.
4 R. Schmuch, R. Wagner, G. Hörpel, T. Placke and M. Winter, *Nat. Energy* 2018, **3**, 267-278.
5 Y. Liu, Y. Zhu and Y. Cui, *Nat. Energy* 2019, **4**, 540-550.
6 C. Wang, T. Liu, X. Yang, S. Ge, N. V. Stanley, E. S. Rountree, Y. Leng and B. D. McCarthy, *Nature* 2022, **611**, 485-490.
7 W. Cai, Y. Yao, G. Zhu, C. Yan, L. Jiang, C. He, J. Huang and Q. Zhang, *Chem. Soc. Rev.* 2020, **49**, 3806-3833.
8 M. Li, J. Lu, Z. Chen and K. Amine, *Adv. Mater.* 2018, **30**, 1800561.
9 Y. Liu, H. Shi and Z. Wu, *Energy Environ. Sci.* 2023, **16**, 4834-4871.
10 C. Zhong, S. Weng, Z. Wang, C. Zhan and X. Wang, *Nano Energy* 2023, **117**, 108894.
11 Y. Tian, Y. An and B. Zhang, *Adv. Energy Mater.* 2023, **13**, 2300123.
12 D. Lin, Y. Liu and Y. Cui, *Nat. Nanotechnol.* 2017, **12**, 194-206.
13 B. T. Heligman, A. Manthiram, *ACS Energy Lett.* 2021, **6**, 2666-2672.
14 P. Li, H. Kim, S. Myung and Y. Sun, *Energy Storage Mater.* 2021, **35**, 550-576.
15 N. Kim, Y. Kim, J. Sung and J. Cho, *Nat. Energy* 2023, **8**, 921-933.
16 A. Li, Z. Wang, T. Lee, N. Zhang, T. Li, W. Zhang, C. Jayawardana, M. Yeddala, B. L. Lucht and C. Wang, *Nat. Energy* 2024, **9**, 1551–1560.
17 J. Liu, Z. Bao, Y. Cui, E. J. Dufek, J. B. Goodenough, P. Khalifah, Q. Li, B. Y. Liaw, P. Liu, A. Manthiram, Y. S. Meng, V. R. Subramanian, M. F. Toney, V. V. Viswanathan, M. S. Whittingham, J. Xiao, W. Xu, J. Yang, X. Yang and J. Zhang, *Nat. Energy* 2019, **4**, 180-186.
18 J. A. Lewis, K. A. Cavallaro, Y. Liu and M. T. McDowell, *Joule* 2022, **6**, 1418-1430.
19 Q. Fang, S. Xu, X. Sha, D. Liu, X. Zhang, W. Li, S. Weng, X. Li, L. Chen, H. Li, B. Wang, Z. Wang and X. Wang, *Energy Environ. Sci.* 2024, **17**, 6368-6376.
20 A. Svirinovsky-Arbeli, M. Juelsholt, R. May, Y. Kwon and L. E. Marbella, *Joule* 2024, **8**, 1919-1935.
21 S. Pan, J. Han, Y. Wang, Z. Li, F. Chen, Y. Guo, Z. Han, K. Xiao, Z. Yu, M. Yu, S. Wu, D. W. Wang and Q. H. Yang, *Adv. Mater.* 2022, **34**, 2203617.
22 T. Liu, T. Dong, M. Wang, X. Du, Y. Sun, G. Xu, H. Zhang, S. Dong and G. Cui, *Nat. Sustain.* 2024, **7**, 1057-1066.
23 S. Li, K. Wang, G. Zhang, S. Li, Y. Xu, X. Zhang, X. Zhang, S. Zheng, X. Sun and Y. Ma, *Adv. Funct. Mater.* 2022, **32**, 2200796.
24 S. Kim, S. Park, M. Kim, Y. Cho, G. Kang, S. Ko, D. Yoon, S. Hong and N. Choi, *Adv. Sci.* 2024, **12**, 2411466.
25 X. He, D. Bresser, S. Passerini, F. Baakes, U.e Krewer, J. Lopez, C. T. Mallia, Y. Shao-Horn, I. Cekic-Laskovic, S. Wiemers-Meyer, F. A. Soto, V. Ponce, J. M. Seminario, P. B. Balbuena, H. Jia, W. Xu, Y. Xu, C. Wang, B. Horstmann, R. Amine, C. Su, J. Shi, K. Amine, M. Winter and R. K. A. Latz, *Nat. Rev. Mater.* 2021, **6**, 1036-1052.
26 H. Wan, J. Xu and C. Wang, *Nat. Rev. Chem.* 2023, **8**, 30-44.
27 J. He, J. Meng and Y. Huang, *J. Power Sources* 2023, **570**, 232965.
28 K. Xu, *J. Power Sources* 2023, **559**, 232652.
29 T. Li, X. Zhang, P. Shi and Q. Zhang, *Joule* 2019, **3**, 2647-2661.
30 Y. Yamada, J. Wang, S. Ko, E. Watanabe and A. Yamada, *Nat. Energy* 2019, **4**, 269-280.
31 C. D. Quilty, D. Wu, W. Li, D. C. Bock, L. Wang, L. M. Housel, A. Abraham, K. J. Takeuchi, A. C. Marschilok and E. S. Takeuchi, *Chem. Rev.* 2023, **123**, 1327-1363.
32 S. Liu, B. Gu, Z. Chen, R. Zhan, X. Wang, R. Feng and Y. Sun, *J. Energy Chem.* 2024, **91**, 484-500.
33 Y. X. Yao, X. Chen, N. Yao, J. H. Gao, G. Xu, J. F. Ding, C. L. Song, W. L. Cai, C. Yan and Q. Zhang, *Angew. Chem.-Int. Edit.* 2022, **62**, e202214828.
34 F. Liu, L. Wang, Z. Zhang, P. Shi, Y. Feng, Y. Yao, S. Ye, H. Wang, X. Wu and Y. Yu, *Adv. Funct. Mater.* 2020, **30**, 2001607.
35 S. Zhang, Y. Zhang, Z. Zhang, H. Wang, Y. Cao, B. Zhang, X. Liu, C. Mao, X. Han, H. Gong, Z. Yang and J. Sun, *Adv. Energy Mater.* 2022, **12**, 2103888.
36 R. Wu, X. Du, T. Liu, X. Zhuang, P. Guan, B. Zhang, S. Zhang, C. Gao, G. Xu, X. Zhou and G. Cui, *Adv. Energy Mater.* 2023, **14**, 2302899.
37 Z. Shi, Y. Wang, X. Yue, J. Zhao, M. Fang, J. Liu, Y. Chen, Y. Dong, X. Yan and Z. Liang, *Adv. Mater.* 2024, **36**, 2401711.

38 Z. Chang, Y. Qiao, H. Deng, H. Yang, P. He and H. Zhou, *Joule* 2020, **4**, 1776-1789.

39 J. Wang, J. Luo, H. Wu, X. Yu, X. Wu, Z. Li, H. Luo, H. Zhang, Y. Hong, Y. Zou, S. Cao, Y. Qiao and S. G. Sun, *Angew. Chem.-Int. Edit.* 2024, **63**, e202400254.

40 C. B. Jin, N. Yao, Y. Xiao, J. Xie, Z. Li, X. Chen, B. Li, X. Q. Zhang, J. Huang and Q. Zhang, **Adv. Mater.** 2022, **35**, 2208340.

41 K. S. Chan, W. Liang and C. K. Chan, *J. Phys. Chem. C* 2019, **123**, 22775-22786.

42 F. Fu, X. Wang, L. Zhang, Y. Yang, J. Chen, B. Xu, C. Ouyang, S. Xu, F. Z. Dai and W. E, *Adv. Funct. Mater.* 2023, **33**, 2303936.

43 Y. Liu, S. Yang, H. Guo, Z. Wang, J. Liu, N. Chen and X. Gong, *Energy Storage Mater.* 2024, **73**, 103806.

44 J. Sun, Y. Li, L. Lv, L. Wang, W. Xiong, L. Huang, Q. Qu, Y. Wang, M. Shen and H. Zheng, *Adv. Funct. Mater.* 2024, **34**, 2410693.

45 Y. Li, B. Wen, N. Li, Y. Zhao, Y. Chen, X. Yin, X. Da, Y. Ouyang, X. Li, P. Kong, S. Ding, K. Xi and G. Gao, *Angew. Chem.-Int. Edit.* 2024, **64**, e202414636.

46 L. Wang, J. Yu, S. Li, F. Xi, W. Ma, K. Wei, J. Lu, Z. Tong, B. Liu and B. Luo, *Energy Storage Mater.* 2024, **66**, 103243.

47 M. Seel, R. Pandey, *Int. J. Quantum Chem.* 1991, **40**, 461-478.

48 K. K. Abady, A. Niksirat, N. Karpourazar and M. Pourfath, presented in part at the 2021 29th Iranian Conference on Electrical Engineering (ICEE), 2021.

49 N. Wu, Y. Li, A. Dolocan, W. Li, H. Xu, B. Xu, N. S. Grundish, Z. Cui, H. Jin and J. B. Goodenough, *Adv. Funct. Mater.* 2020, **30**, 2000831.

50 X. Chen, G. Ge, W. Wang, B. Zhang, J. Jiang, X. Yang, Y. Li, L. Wang, X. He and Y. Sun, *Sci. China-Chem.* 2021, **64**, 1417-1425.

51 H. Wang, H. Man, J. Yang, J. Zang, R. Che, F. Wang, D. Sun and F. Fang, *Adv. Funct. Mater.* 2021, **32**, 2109887.

52 B. Xiang, Y. Liu, S. Mei, Z. Li, S. Guo, X. Guo, Z. Jia, Y. She, J. Fu, P. K. Chu, K. Huo and B. Gao, *Energy Storage Mater.* 2024, **69**, 103416.

53 J. Lee, Y. Ko, M. Shin, H. Song, N. Choi, M. G. Kim and S. Park, *Energy Environ. Sci.* 2015, **8**, 2075-2084.

54 N. Li, Y. Yin, C Yang, Y Guo, *Adv. Mater.* 2015, **28**, 1853-1858.

55 A. Hu, W. Chen, X. Du, Y. Hu, T. Lei, H. Wang, L. Xue, Y. Li, H. Sun, Y. Yan, J. Long, C. Shu, J. Zhu, B. Li, X. Wang and J. Xiong, *Energy Environ. Sci.* 2021, **14**, 4115-4124.

56 X. Jin, Z. Cai, X. Zhang, J. Yu, Q. He, Z. Lu, M. Dahbi, J. Alami, J. Lu, K. Amine and H. Zhang, *Adv. Mater.* 2022, **34**, 2200181.

57 X. Liang, Q. Pang, I. R. Kochetkov, M. S. Sempere, H. Huang, X. Sun and L. F. Nazar, *Nat. Energy* 2017, **2**, 17119.

58 M. Niu, L. Dong, J. Yue, Y. Li, Y. Dong, S. Cheng, S. Lv, Y. H. Zhu, Z. Lei, J. Y. Liang, S. Xin, C. Yang and Y. G. Guo, *Angew. Chem.-Int. Edit.* 2024, **63**, e202318663.

59 J. H. Choi, H. G. Lee, M. H. Lee, S. M. Lee, J. Kang, J. H. Suh, M. S. Park and J. W. Lee, *Adv. Funct. Mater.* 2024, **34**, 2400414.

60 Y. Lin, F. Su, J. Jiang, H. You, M. Yao, C. Lian, L. Chen, H. Liu and C. Li, *Energy Storage Mater.* 2024, **70**, 103484.

61 Y. Wang, T. Li, X. Yang, Q. Yin, S. Wang, H. Zhang and X. Li, *Adv. Energy Mater.* 2023, **14**, 2303189.

62 S. Tu, B. Zhang, Y. Zhang, Z. Chen, X. Wang, R. Zhan, Y. Ou, W. Wang, X. Liu, X. Duan, L. Wang and Y. Sun, *Nat. Energy* 2023, **8**, 1365-1374.

63 Y. Huang, C. Wang, H. Lv, Y. Xie, S. Zhou, Y. Ye, E. Zhou, T. Zhu, H. Xie, W. Jiang, X. Wu, X. Kong, H. Jin and H. Ji, *Adv. Mater.* 2023, **36**, 2308675.

64 C. Wang, Y. Xie, Y. Huang, S. Zhou, H. Xie, H. Jin and H. Ji, *Angew. Chem.-Int. Edit.* 2024, **63**, 2402077.

65 K. Cheng, S. Tu, B. Zhang, W. Wang, X. Wang, Y. Tan, X. Chen, C. Li, C. Li, L. Wang and Y. Sun, *Energy Environ. Sci.* 2024, **17**, 2631-2641.

66 S. Weng, X. Zhang, G. Yang, S. Zhang, B. Ma, Q. Liu, Y. Liu, C. Peng, H. Chen, H. Yu, X. Fan, T. Cheng, L. Chen, Y. Li, Z. Wang and X. Wang, *Nat. Commun.* 2023, **14**, 4474.

67 Y. Mo, G. Liu, J. Chen, X. Zhu, Y. Peng, Y. Wang, C. Wang, X. Dong and Y. Xia, *Energy Environ. Sci.* 2024, **17**, 227-237.

68 H. Lim, D. T. Nguyen, J. A. Lochala, X. Cao and J. Zhang, *ACS Energy Lett.* 2023, **9**, 126-135.

69 W. Liu, Y. Luo, Y. Hu, Z. Chen, Q. Wang, Y. Chen, N. Iqbal and D. Mitlin, *Adv. Energy Mater.* 2023, **14**, 2302261.

70 Y. Sun, L. Wang, Y. Li, Y. Li, H. R. Lee, A. Pei, X. He and Y. Cui, *Joule* 2019, **3**, 1080-1093.

71 N. Liu, Z. Lu, J. Zhao, M. T. McDowell, H.-W. Lee, W. Zhao and Y. Cui, *Nat. Nanotechnol.* 2014, **9**, 187-192.

72 M. Ko, S. Chae, J. Ma, N. Kim, H. Lee, Y. Cui and J. Cho, *Nat. Energy* 2016, **1**, 16113.

73 B. Wang, J. Ryu, S. Choi, X. Zhang, D. Pribat, X. Li, L. Zhi, S. Park and R. S. Ruoff, *ACS Nano* 2019, **13**, 2307-2315.

74 L. Zhang, C. Wang, Y. Dou, N. Cheng, D. Cui, Y. Du, P. Liu, M. Al‐Mamun, S. Zhang and H. Zhao, *Angew. Chem.-Int. Edit.* 2019, **58**, 8824-8828.

75 J. Ma, J. Sung, Y. Lee, Y. Son, S. Chae, N. Kim, S. H. Choi and J. Cho, *Adv. Energy Mater.* 2019, **10**, 1903400.

76 Z. Zhao, J. Han, F. Chen, J. Xiao, Y. Zhao, Y. Zhang, D. Kong, Z. Weng, S. Wu and Q. H. Yang, *Adv. Energy Mater.* 2022, **12**, 2103565.

77 S. Sun, C. Wang, M. Chen, M. Li and L. Wang, *J. Colloid Interface Sci.* 2014, **426**, 206-208.

78 S. Yang, H. Song and X. Chen, *Carbon* 2006, **44**, 730-733.

79 S. Tu, Z. Lu, M. Zheng, Z. Chen, X. Wang, Z. Cai, C. Chen, L. Wang, C. Li, Z. W. Seh, S. Zhang, J. Lu and Y. Sun, *Adv. Mater.* 2022, **34**, 2202892.

80 S. Ahmed, I. Bloom, A. N. Jansen, T. Tanim, E. J. Dufek, A. Pesaran, A. Burnham, R. B. Carlson, F. Dias, K. Hardy, M. Keyser, C. Kreuzer, A. Markel, A. Meintz, C. Michelbacher, M. Mohanpurkar, P. A. Nelson, D. C. Robertson, D. Scoffield, M. Shirk, T. Stephens, R. Vijayagopal and J. Zhang, *J. Power Sources* 2017, **367**, 250-262.

81 K. G. Gallagher, S. E. Trask, C. Bauer, T. Woehrle, S. F. Lux, M. Tschech, P. Lamp, B. J. Polzin, S. Ha, B. Long, Q. Wu, W. Lu, D. W. Dees and A. N. Jansen, *J. Electrochem. Soc.* 2015, **163**, A138-A149.

82 Z. Yan, L. Wang, H. Zhang and X. He, *Adv. Energy Mater.* 2024, **14**, 2303206.

83 J. Billaud, F. Bouville, T. Magrini, C. Villevieille and A. R. Studart, *Nat. Energy* 2016, **1**, 16097.

84 K. Chen, M. J. Namkoong, V. Goel, C. Yang, S. Kazemiabnavi, S. M. Mortuza, E. Kazyak, J. Mazumder, K. Thornton, J. Sakamoto and N. P. Dasgupta, *J. Power Sources* 2020, **471**, 228475.

85 D. Parikh, J. Li, *Carbon* 2022, **196**, 525-531.

86 M. Doyle, T. F. Fuller and J. Newman, *Electrochim. Acta* 1994, **39**, 2073-2081.

87 K. M. Diederichsen, E. J. McShane and B. D. McCloskey, *ACS Energy Lett.* 2017, **2**, 2563-2575.

88 J. B. Park, C. Choi, S. Yu, K. Y. Chung and D. W. Kim, *Adv. Energy Mater.* 2021, **11**, 2101544.

89 Z. Yu, H. Wang, X. Kong, W. Huang, Y. Tsao, D. G. Mackanic, K. Wang, X. Wang, W. Huang, S. Choudhury, Y. Zheng, C. V. Amanchukwu, S. T. Hung, Y. Ma, E. G. Lomeli, J. Qin, Y. Cui and Z. Bao, *Nat. Energy* 2020, **5**, 526-533.

90 Z. Yu, P. E. Rudnicki, Z. Zhang, Z. Huang, H. Celik, S. T. Oyakhire, Y. Chen, X. Kong, S. C. Kim, X. Xiao, H. Wang, Y. Zheng, G. A. Kamat, M. S. Kim, S. F. Bent, J. Qin, Y. Cui and Z. Bao, *Nat. Energy* 2022, **7**, 94-106.

91 J. Lau, R. H. DeBlock, D. M. Butts, D. S. Ashby, C. S. Choi and B. S. Dunn, *Adv. Energy Mater.* 2018, **8**, 1800933.

92 J. Evans, C. A. Vincent and P. G. Bruce, *Polymer* 1987, **28**, 2324-2328.

93 S. Tu, Y. Zhang, D. Ren, Z. Chen, W. Wang, R. Zhan, X. Wang, K. Cheng, Y. Ou, X. Duan, L. Wang and Y. Sun, *Adv. Funct. Mater.* 2024, **34**, 2402077.

View Article Online
DOI: 10.1039/D4EE06107A

94 Y. Xia, P. Zhou, X. Kong, J. Tian, W. Zhang, S. Yan, W. Hou, H. Zhou, H. Dong, X. Chen, P. Wang, Z. Xu, L. Wan, B. Wang and K. Liu, *Nat. Energy* 2023, **8**, 934-945.

95 X. B. Cheng, R. Zhang, C. Z. Zhao and Q. Zhang, *Chem. Rev.* 2017, **117**, 10403-10473.

96 M. Fang, X. Yue, Y. Dong, Y. Chen and Z. Liang, *Joule* 2024, **8**, 91-103.

97 M. Wan, S. Kang, L. Wang, H. W. Lee, G. W. Zheng, Y. Cui and Y. Sun, *Nat. Commun.* 2020, **11**, 829.

98 J. Cao, Y. Shi, A. Gao, G. Du, M. Dilxat, Y. Zhang, M. Cai, G. Qian, X. Lu, F. Xie, Y. Sun and X. Lu, *Nat. Commun.* 2024, **15**, 1354.

99 D. Jin, Y. Roh, T. Jo, M. H. Ryou, H. Lee and Y. M. Lee, *Adv. Energy Mater.* 2021, **11**, 2003769.

100 G. Li, X. Duan, X. Liu, R. Zhan, X. Wang, J. Du, Z. Chen, Y. Li, Z. Cai, Y. Shen and Y. Sun, *Adv. Mater.* 2023, **35**, 2207310.

101 L. Cao, M. Chu, Y. Li, X. Xu, Y. Qiu, Y. Dai, C. Sun, Z. X. Huang, X. L. Wu and H. Geng, *Adv. Mater.* 2024, **36**, 246034.

102 L. Wang, X. Wang, R. Zhan, Z. Chen, S. Tu, C. Li, X. Liu, Z. W. Seh and Y. Sun, *ACS Appl. Mater. Interfaces* 2022, **14**, 37709-37715.

103 C. Zhang, H. Fan, X. Chen, H. Xu, J. Lou, Y. Li, Y. Huang and S. Li, *Energy Environ. Sci.* 2022, **15**, 5251-5260.

104 H. Chen, Y. Yang, D. T. Boyle, Y. K. Jeong, R. Xu, L. S. de Vasconcelos, Z. Huang, H. Wang, H. Wang, W. Huang, H. Li, J. Wang, H. Gu, R. Matsumoto, K. Motohashi, Y. Nakayama, K. Zhao and Y. Cui, *Nat. Energy* 2021, **6**, 790-798.

105 L. Fu, X. Wang, B. Zhang, Z. Chen, Y. Li and Y. Sun, *Nano Res.* 2024, **17**, 4031-4038.

106 X. Wu, W. Zhang, N. Wu, S. S. Pang, Y. Ding and G. He, *Adv. Energy Mater.* 2021, **11**, 2003082.

107 Z. Guo, T. Wang, D. Wang, H. Xu, X. Liu, Y. Dai, H. Yang, Y. Huang and W. Luo, *ACS Nano* 2023, **17**, 14136-14143.

View Article Online
DOI: 10.1039/D4EE06107A

Data Availability Statement

The data that support the findings of this study are available from the corresponding author upon reasonable request.